

ESA Cloud_cci+

Final Report - Phase 1 (2020-2023)



Issue 1 Revision 0

23/01/2024

Deliverable No.: D-6.2

ESRIN/Contract No.: 4000128637/20/I-NB

Science lead: Dr. Martin Stengel

Deutscher Wetterdienst martin.stengel@dwd.de

Technical Officer: Michael Eisinger

European Space Agency Michael. Eisinger@esa.int





Doc:		Cloud_cci+_D6.2_FINAL_REPORT_Phase1_v1.0.docx				
Date:				23/01/2024		
Issue:	1	Revision:	0	Page 2		

Document Change Record

Document, Version	Date	Changes	Originator
v1.0	23/01/2024	final version	Martin Stengel

Purpose of this Document

The purpose of this document is to report a concise and complete description of all the work done during the Cloud_cci+ phase 1. It is meant to be self-standing, not requiring to be read in conjunction with reports previously issued. This report summarizes all major activities performed and the main results achieved. It gives link for further readings whenever possible and needed.



Doc:			Cloud_cci+	_D6.2_FINAL_REPORT_Phase1_v1.0.docx
Date:				23/01/2024
Issue:	1	Revision:	0	Page 3

Contents

EXECUTI	VE SUMMARY 5
1 INTR	ODUCTION ϵ
1.1 Th	e ESA Cloud_cci+ project6
1.2 Clc	oud_cci+ cloud and radiative flux properties6
2 DATA	ASETS AND EVALUATION 8
2.1 Da	tasets 8
2.2 Eva	aluation13
3 ACC(OMPANYING ACTIVITIES15
3.1 Sat 3.1.1 3.1.2 3.1.3	tellite simulator
3.2 Un 3.2.1 3.2.2	certainty analysis & characterization
4 USER	R CASE STUDIES23
Radiativ 4.1.1	er Case Study I - A Lagrangian Perspective on the Lifecycle and Cloud e Effect of Deep Convective Clouds Over Africa
	er Case Study II - Designing a 'Sunny Vacation Map' based on Satellite tions on Clouds and Radiation25
4.2.1	Scope
4.2.2	
	Approach
cloud pr	ngular Vector Decomposition (SVD) of satellite datasets: relation betweer coperties and climate indices



Doc:			Cloud_cci+	_D6.2_FINAL_REPORT_Phase1_v1.0.docx
Date:				23/01/2024
Issue:	1	Revision:	0	Page 4

		Method Conclusions	
5	REFE	RENCES	30
6	DEFI	NITIONS, ACRONYMS, ABBREVIATIONS	32
14	NNEX A	- ARCHITECTURE OF THE CLOUD CCI PROCESSING ENVIRONMENT	34



Doc:		Cloud_cci+_D6.2_FINAL_REPORT_Phase1_v1.0.docx				
Date:				23/01/2024		
Issue:	1	Revision:	0	Page 5		

Executive Summary

In Phase I of the ESA Cloud_cci+ project two demonstrator datasets were generated covering the year 2019. One dataset is based on measurements from the Spinning Enhances Visible and IR Imager (SEVIRI) on board the Meteosat Second Generation (MSG) satellites. The other dataset is based on measurements from the SLSTR sensor on board the Sentinel 3a and 3b satellites. Both datasets were generated by employing the Community Cloud retrieval for Climate (CC4CL) and contain a comprehensive set of cloud and radiative flux properties. The datasets were comprehensively documented (e.g. Algorithm Theoretical Baseline Document, Product Validation and Intercomparison Report, Product User Guide). In addition, a satellite simulator, that was developed in a previous project phase, was extended to be representative for SLSTR, which eases comparisons between the SLSTR datasets and model output when post-processed with that simulator. Furthermore, some effort was put in analysing and describing the uncertainties associated with the generated data, including the role of errors in the ancillary data and uncertainties introduced by limited spectral information and limited temporal sampling. Two User Case Studies were conducted in this project phase. One study was on the lifecycles of the cloud radiative effect of deep convective systems over Africa. This study made use of cloud and radiative flux properties available from temporally highly resolved SEVIRI data. The second study focussed on analysing cloud and radiative flux data for processing the spatially-resolved likelihood of sunny days and sunny periods. With this as input sunny vacation maps were derived. The study used primarily AVHRR data that were generated in a previous project phase. Using the ATSR2-AATSR data of the previous project phase, another study developed a singular vector decomposition technique to describe spatial patterns of temporal variability of cloud properties and these coincide with for example ENSO indices.



Doc:		Cloud_cci+_D6.2_FINAL_REPORT_Phase1_v1.0.docx				
Date:				23/01/2024		
Issue:	1	Revision:	0	Page 6		

1 Introduction

1.1 The ESA Cloud_cci+ project

The Cloud_cci+ project contributes to and improves on the successful efforts of Cloud_cci: the development, validation and application of novel cloud property data sets maximising the use of ESA and other European EO mission data and targeting the GCOS requirements for the Cloud ECV. The Cloud_cci+ project phase I was kicked off in March 2020 and ended in Dec 2023.

Cloud_cci+ Phase I

The goal of the ESA Cloud_cci+ has been the improvement of retrieval algorithms and processing concepts and implementations, and the development of two demonstrator data sets based on measurements form the Spinning Enhances Visible and Infrared Imager (SEVIRI) and from the Sea and Land Surface Temperature Radiometer (SLSTR). The processing systems have the potential to be used for a sustained data production in operational entities, for instance the EUMETSAT SAF network and the Copernicus Climate Change Service, after the current R&D under the ESA CCI programme has been completed.

A full list of planned and carried out CC4CL developments in Cloud_cci+ Phase I is given in the Algorithm Development Plan (ADPv3.0). The cloud products retrieved from SEVIRI and SLSTR remain the same compared to previous datasets and are outlined in the next subsection. The SEVIRI and SLSTR data cover the year 2019 and include the cloud products presented in the next subsection. Examples are shown in Figure 1-1.

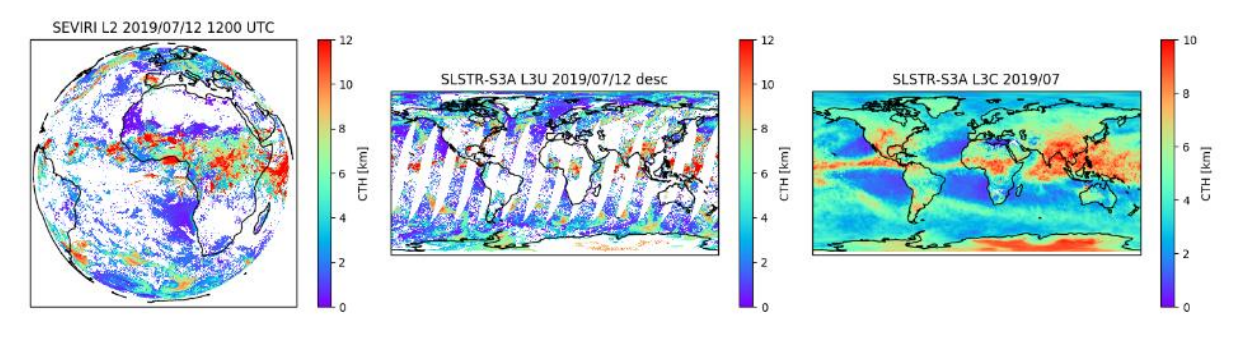


Figure 1-1 Examples of Level-2 cloud top height fields from SEVIRI (left) and SLSTR-S3a (middle). Right panel depicts an example monthly mean cloud top height field from SLSTR-S3a.

1.2 Cloud cci+ cloud and radiative flux properties

The cloud properties derived on satellite pixel level of each utilized sensor are listed in Table 1-1. Primarily retrieved cloud properties are CMA/CFC, CPH, CTP, COT and CER. The properties CLA, LWP, IWP are determined from retrieved COT and CER in a post processing step. The same applies to CTH and CTT, which are inferred from the retrieved CTP. Radiative fluxes properties are calculated using radiative transfer calculation (requiring ERA5 data) ingesting the retrieved cloud properties. Based on the pixel level retrievals the data is further processed into different processing levels as summarized in Table 2-2. Level-3U denotes a global composite on a global Latitude-Longitude grid (of 0.05° resolution) onto which the Level-2 data is sampled. Level-3C products are also defined on Latitude-Longitude grid (0.5° resolution) onto which the properties are averaged and their frequency collected (histograms). Further separation of cloud properties in Level-3C in e.g. day/night, liquid/ice, were made wherever suitable (see



Doc:		C	loud_cci+	_D6.2_FINAL_REPORT_Phase1_v1.0.docx
Date:				23/01/2024
Issue:	1	Revision:	0	Page 7

Table 2-3). The reader is referred to ATBDv9.0 for more details on Level-3U and Level-3C generation).

Table 1-1 List of generated cloud properties. CMA/CFC and CPH are derived in a pre-processing step using Artificial Neural Networks. In the next step, COT, CER and CTP are retrieved simultaneously by fitting a physically consistent cloud/atmosphere/surface model to the satellite observations using optimal estimation (OE). Moreover, LWP and IWP are obtained from COT and CER. In addition, spectral cloud albedo (CLA) for two visible channels are derived. In a post-processing step, derived cloud properties and ERA-Interim information are used to determine radiative broadband fluxes.

Variable	Abbrev.	Definition
Cloud mask / Cloud fraction	CMA/ CFC	A binary cloud mask per pixel (L2, L3U) and therefrom derived monthly total cloud fractional coverage (L3C) and separation into 3 vertical classes (high, mid-level, low clouds) following ISCCP classification (Rossow and Schiffer, 1999).
Cloud phase	СРН	The thermodynamic phase of the retrieved cloud (binary: liquid or ice; in L2, L3U) and the therefrom derived monthly liquid cloud fraction (L3C).
Cloud optical thickness	СОТ	The line integral of the absorption coefficient and the scattering coefficient (at 0.55µm wavelength) along the vertical in cloudy pixels.
Cloud effective radius	CER	The area-weighted radius of the cloud drop and crystal particles, respectively.
Cloud top pressure/ height/ temperature	CTP/ CTH/ CTT	The air pressure [hPa] /height [m] /temperature [K] of the uppermost cloud layer that could be identified by the retrieval system.
Cloud liquid water path/ Ice water path	LWP/ IWP	The vertical integrated liquid/ice water content of existing cloud layers; derived from CER and COT. LWP and IWP together represent the cloud water path (CWP)
Joint cloud property histogram	JCH	This product is a spatially resolved two-dimensional histogram of combinations of COT and CTP for each spatial grid box.
Spectral cloud albedo	CLA	The blacksky cloud albedo derived for channel 1 (0.67 μ m) and 2 (0.87 μ m), respectively (experimental product)
Cloud effective emissivity	CEE	cloud radiative thickness in the infrared typically referred to as the "effective emissivity"
Top of atmosphere upwards/downwards flux	TOA	Shortwave (SW) and longwave (LW) fluxes at the Top of the atmosphere, upwelling and downwelling
Top of atmosphere upwards/downwards flux - clear-sky	TOA _{clear}	Shortwave (SW) and longwave (LW) fluxes at the Top of the atmosphere, upwelling and downwelling - for clear sky conditions
Bottom of atmosphere (surface) upwards/downwards flux	ВОА	Shortwave (SW) and longwave (LW) fluxes at the Bottom of the atmosphere, upwelling and downwelling
Bottom of atmosphere (surface) upwards/downwards flux - clear-sky	BOA _{clear}	Shortwave (SW) and longwave (LW) fluxes at the Bottom of the atmosphere, upwelling and downwelling - for clear sky conditions



Doc:			Cloud_cci+	_D6.2_FINAL_REPORT_Phase1_v1.0.docx
Date:				23/01/2024
Issue:	1	Revision:	0	Page 8

2 Datasets and Evaluation

2.1 Datasets

Cloud_cci+ generated 3 version of SEVIRI and SLSTR demonstrator datasets. While the first two versions were limited to February and July 2019, the final demonstrator data (version 3) covered all months in 2019. The remaining discussion in this section addresses the version 3 data.

The Cloud_cci+ v3 datasets for SLSTR and SEVIRI are summarized in Table 2-1 and include the cloud and radiative flux properties listed Table 1-1. For both datasets the Community Cloud retrieval for Climate (CC4CL; McGarragh et al., 2017 and Sus et al., 2017) systems was used with latest developments given in ATBDv9.0, ATBD-CC4CLv9.0 and ATBD-CC4CL-TOAFLUXv1.1. Both datasets include multiple processing levels ranging from pixel-level data (Level-2) for SEVIR and SLSTR, over global daily composites (Level-3U) for SLSTR to monthly averages and histograms (Level-3C) for SEVIRI and SLSTR. The processing levels are summarized in Table 2-2 and



Doc:			Cloud_cci+	_D6.2_FINAL_REPORT_Phase1_v1.0.docx
Date:				23/01/2024
Issue:	1	Revision:	0	Page 9

Table 2-3.

Figure 2-1 toFigure 2-2Figure 2-3 show examples of Cloud_cci+ Phase 1 products for cloud mask/fraction and TOA upwelling short and longwave radiation. A complete product description is given in PUGv1.

Table 2-1 Details and processing status of Cloud_cci+ Climate Research Data Package (CRDP) v3.

Data	Sensor	Satellite(s)	Time period	Algorithm	Processing levels
Cloud_cci+ SEVIRI	SEVIRI	MSG-2/4	2019 all months	CC4CL	L2*, L3C
Cloud_cci+ SLSTR	SLSTR	Sentinel-3a/b	2019 all months	CC4CL	L2, L3U, L3C

^{*}Additional SEVIRI L2 data for July 2019 exist based on CC4CL multi-layer mode retrievals

Table 2-2 Processing levels of Cloud_cci+ data products. Level-3U and Level-3C are each directly derived from Level-2.

Processing level	Spatial resolution	Description			
Level-2 (L2)	SLSTR: 1km SEVIRI: 3-5 km	Retrieved cloud variables at satellite sensor pixel level, thus with the same resolution and location as the sensor measurements (Level-1)			
Level-3U* (L3U)	Latitude-Longitude grid at 0.05° res.	Cloud properties of Level-2 orbits projected onto a global space grid without combining any observations of overlapping orbits. Only subsampling is done. Common notation for this processing level is also L2b. Temporal coverage is 24 hours (0-23:59 UTC).			
Level-3C (L3C) Latitude-Longitude grid at 0.5° res. Cloud properties of Level-2 orbits of one single sensor combined (averaged / sampled for histograms) on a global space grid. Temporal coverage of this product is 1 month.					
* Level-3U dat	a are only provided for S	LSTR and not for SEVIRI products			



Doc:			Cloud_cci+	_D6.2_FINAL_REPORT_Phase1_v1.0.docx
Date:				23/01/2024
Issue:	1	Revision:	0	Page 10

Table 2-3 Cloud_cci+ product features incl. day and night separation, liquid water and ice as well as histogram representation. Level-3U refers to the un-averaged, pixel-based cloud retrievals sampled onto a global Latitude-Longitude (lat/lon) grid. ¹CMA in Level-2 and Level-3U is a binary cloud mask. All products listed exist in each dataset listed above.

Level 2 Level-3U* Level-3C Level-3C swath based daily sampled monthly averages monthly histograms global global global 1km/5km 0.5° lat/lon grid 0.05° lat/lon grid 0.5° lat/lon grid √day/night/high/mid/low ✓ as CMA¹ ✓ as CMA¹ CMA/CFC CTP, CTH, CTT √ liquid/ice CPH √ day/night COT √ liquid/ice √ liquid/ice **CER** √ liquid/ice √ liquid/ice **LWP** ✓ as CWP ✓ as CWP ✓ as CWP **IWP** ✓ **√** 0.6/0.8µm **✓** 0.6/0.8µm CLA ✓ 0.6/0.8µm 0.6/0.8µm/liquid/ice √ liquid/ice **JCH** ✓ $\textbf{TOA}_{up,dn,sw,lw}$ **BOA**_{up,dn,sw,lw}

^{*} Level-3U data are only provided for SLSTR and not for SEVIRI products



Doc:			Cloud_cci+	_D6.2_FINAL_REPORT_Phase1_v1.0.docx
Date:				23/01/2024
Issue:	1	Revision:	0	Page 11

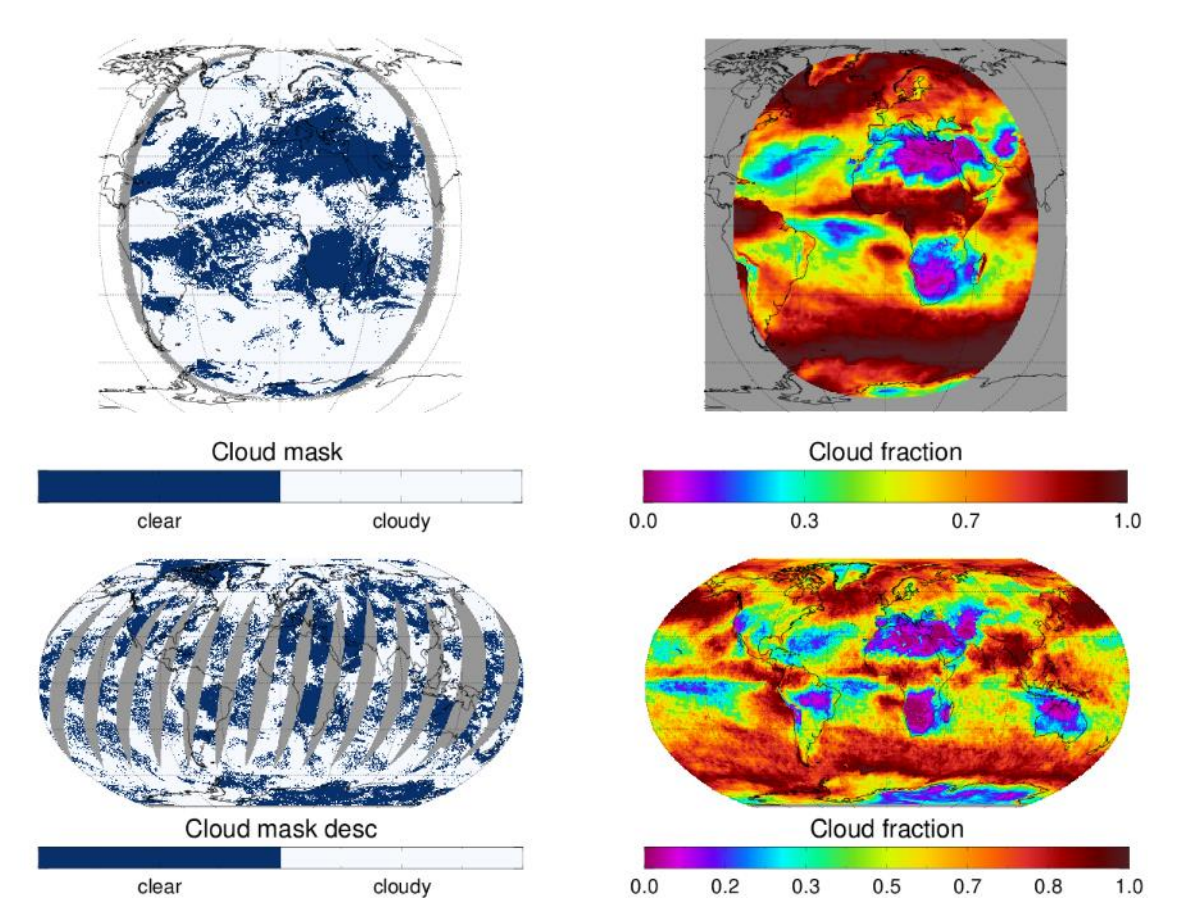


Figure 2-1 Top row: Map of Cloud_cci SEVIRI L2 cloud mask for 2019/07/01 12 UTC (left) and map of Cloud_cci SEVIRI L3C monthly mean total cloud fraction for 2019/07 (right). Bottom row: Map of Cloud_cci SLSTR S3a L3U cloud mask for 2019/07/01 (left) and map of Cloud_cci SLSTR S3a L3C monthly mean total cloud fraction for 2019/07 (right). Figure taken from PUGv1.



Doc:			Cloud_cci+	_D6.2_FINAL_REPORT_Phase1_v1.0.docx
Date:				23/01/2024
Issue:	1	Revision:	0	Page 12

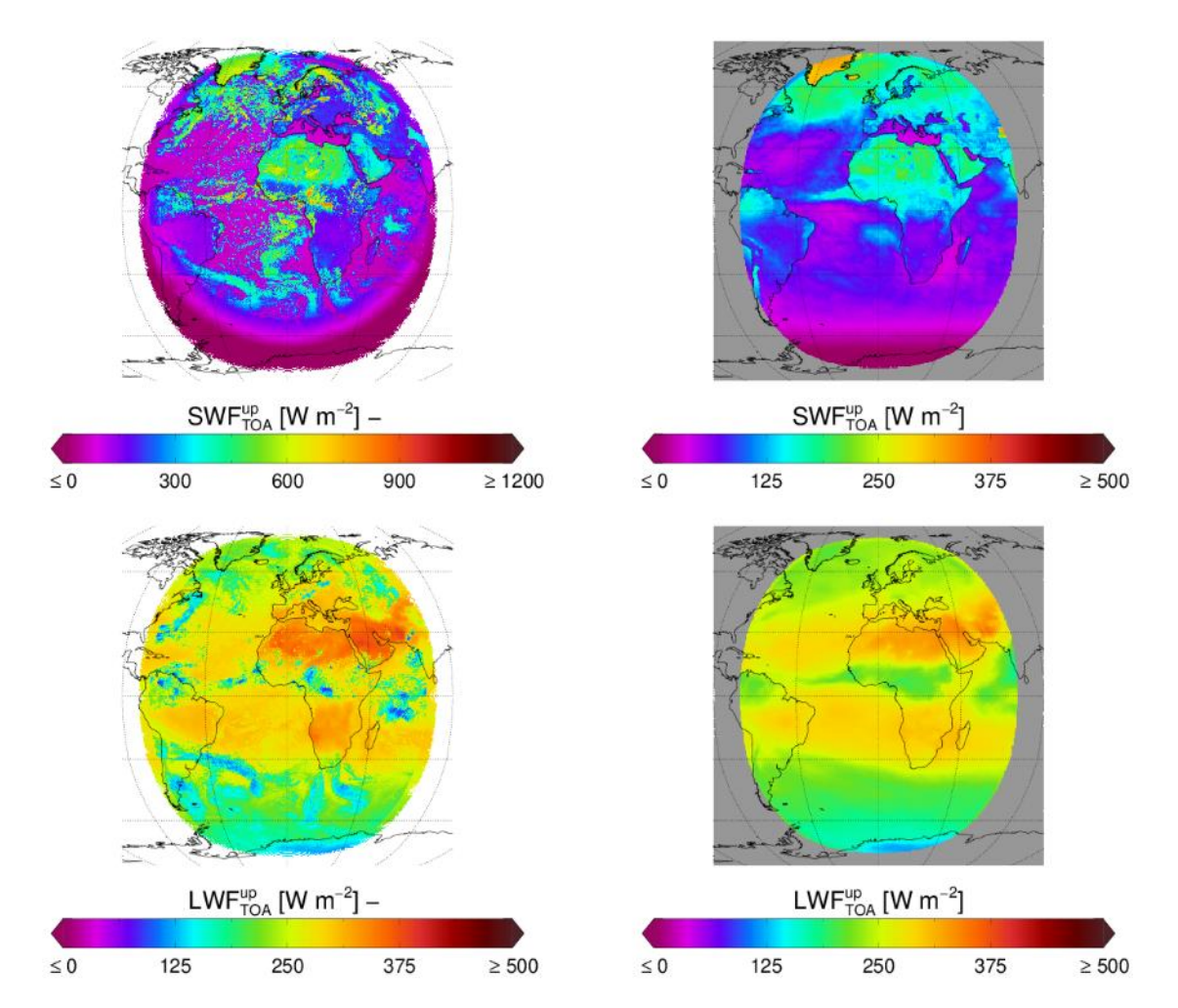


Figure 2-2 Left column: Maps of Cloud_cci SEVIRI L2 upwelling shortwave (top) and longwave (bottom) broadband flux at top of the atmosphere (SWF_{TOA}^{up} , LWF_{TOA}^{up}) for 2019/07/01 12 UTC. Right column: Maps of Cloud_cci SEVIRI L3C monthly mean upwelling shortwave (top) and longwave (bottom) broadband flux at top of the atmosphere for 2019/07. Figure taken from PUGv1.



Doc:			Cloud_cci+	_D6.2_FINAL_REPORT_Phase1_v1.0.docx
Date:				23/01/2024
Issue:	1	Revision:	0	Page 13

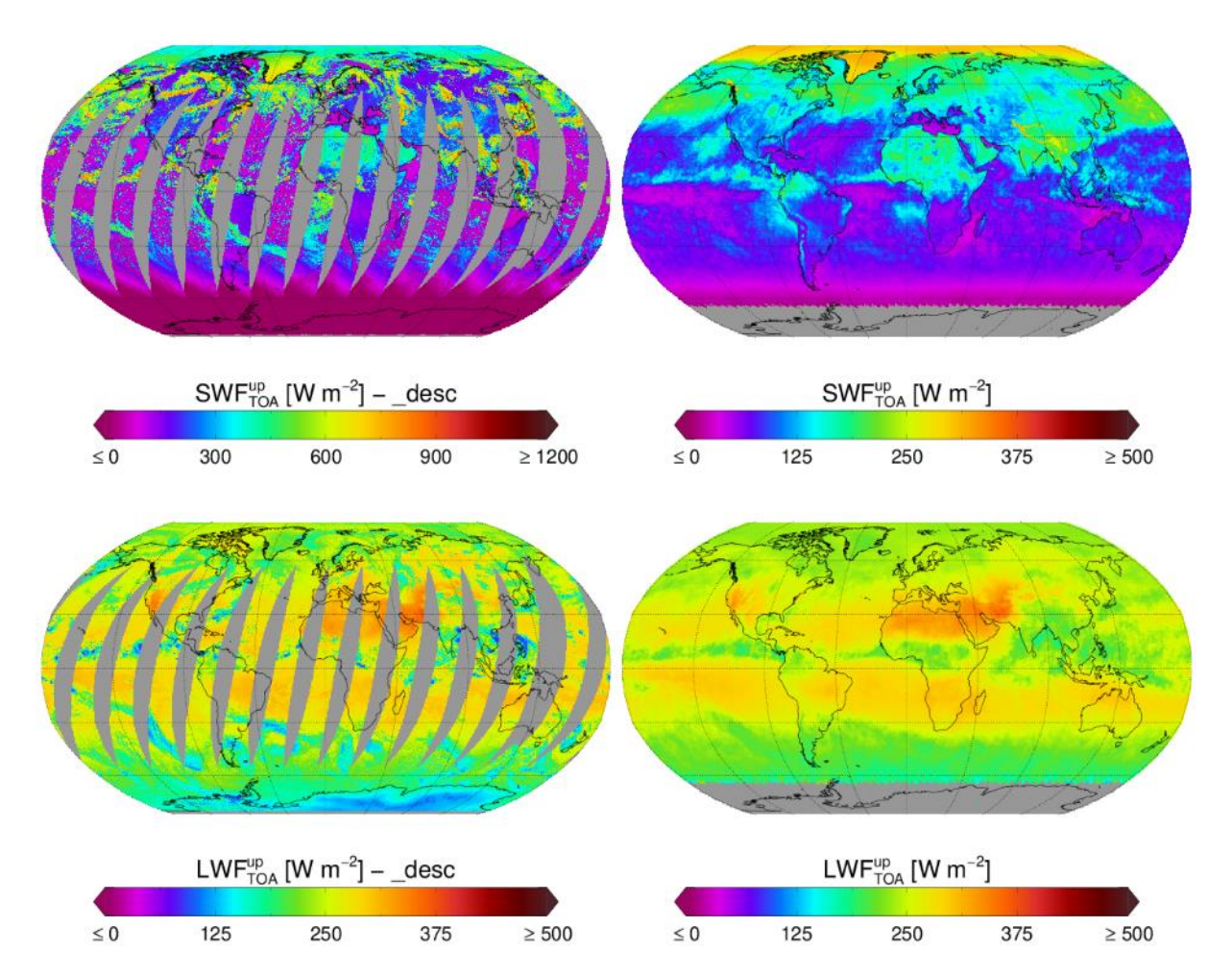


Figure 2-3 Left column: Maps of Cloud_cci SLSTR S3a L3U upwelling shortwave (top) and longwave (bottom) broadband flux at top of the atmosphere (SWF_{TOA}^{up} , LWF_{TOA}^{up}) for 2019/07/01 12 UTC. Right column: Maps of Cloud_cci SLSTR S3a L3C monthly mean upwelling shortwave (top) and longwave (bottom) broadband flux at top of the atmosphere for 2019/07. Figure taken from PUGv1.



Doc:			Cloud_cci+	D6.2_FINAL_REPORT_Phase1_v1.0.docx
Date:				23/01/2024
Issue:	1	Revision:	0	Page 14

2.2 Evaluation

As part of a thorough characterization of all Cloud_cci+ generated demonstrator datasets, comprehensive validation efforts were undertaken, which included:

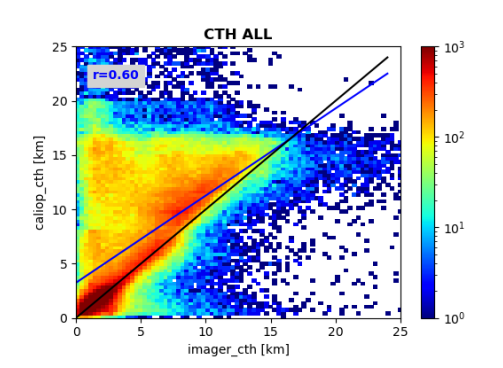
- Validation of cloud mask, phase and height against the active, space-based Lidar CALIOP
- Validation of liquid water path against passive microwave LWP products
- Validation of ice water path against active, space-based Lidar-Radar products of DARDAR.

with Figure 2-5 presenting example validation results for CTH and LWP. All individual validation scores are details in PVIRv2.0 (version 2 data) and PVIRv3.0 (version 3 (final) data).

Additionally, comparisons of Cloud_cci+ datasets with well-established cloud climatologies were conducted using:

- MODIS Collection 6.1 for comparisons with SLSTR and
- CM SAF CLAAS-3 data for comparisons with SEVIRI.

Furthermore, the evaluation additionally included comparisons against well-established radiative flux products of CERES for TOA fluxes. Ground based in-situ observations of SYNOP stations and of BSRN stations were used to validate monthly cloud cover and monthly mean downwelling radiative fluxes at BOA. Example comparisons for SLSTR S3A monthly mean CFC and TOA upwelling shortwave flux are shown in Figure 2-6.



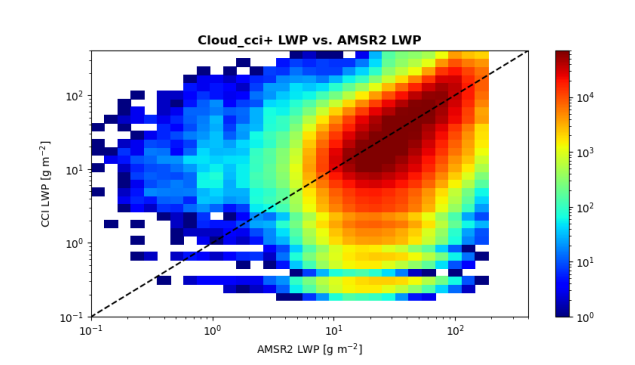
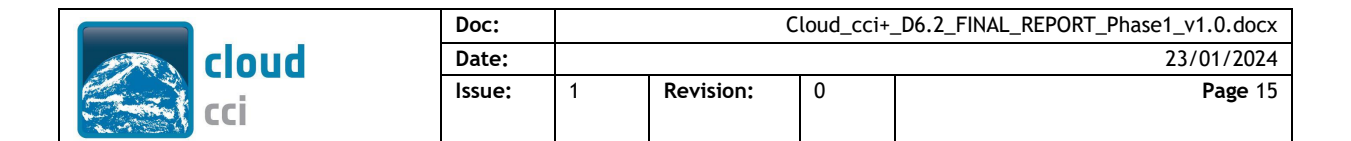


Figure 2-4

Figure 2-5 Left: Two-dimensional histogram of Cloud_cci SEVIRI CTH (x-axis) and CALIOP CTH (y-axis). Black line is the 1:1 line and blue line indicates the linear regression line. Right: Validation results of Cloud_cci SEVIRI and AMSR2 liquid water path (LWP): 2-dimensional histogram of AMSR2 LWP (x-axis) vs. Cloud_cci SEVIRI LWP (y-axis) using a log-log scale. Bin size is 5x5 g m-2. Black dashed line is the 1:1 line. Results taken from PVIRv3.0.



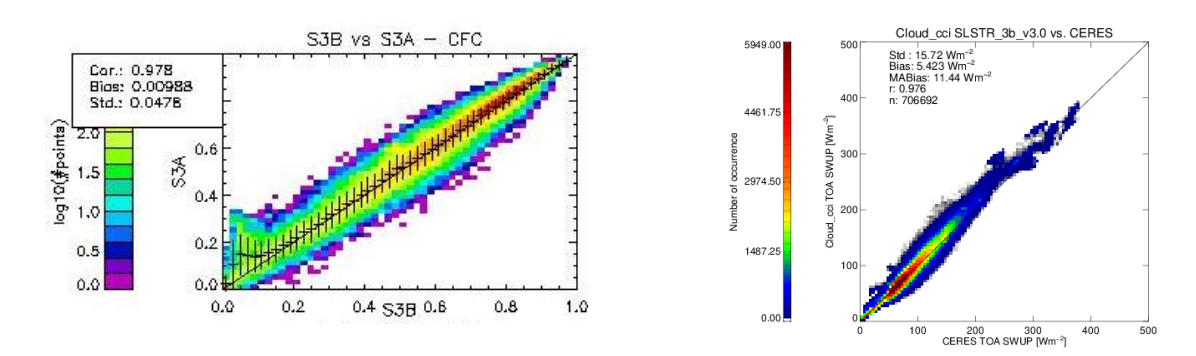


Figure 2-6 Left: Density scatter plot between monthly mean Cloud_cci S3A CFC and MODIS for Feb 2019). Right: Density scatter plot of monthly mean Cloud_cci SLSTR S3b TOA upwelling shortwave flux compared to CERES EBAF-TOA Ed4.0 all months in 2019. Results taken from PVIRv3.0.



Doc:			Cloud_cci+	_D6.2_FINAL_REPORT_Phase1_v1.0.docx
Date:				23/01/2024
Issue:	1	Revision:	0	Page 16

3 Accompanying activities

3.1 Satellite simulator

3.1.1 Simplistic cloud simulator for ERA-Interim

A full and peer-reviewed description of the simplistic cloud simulator is given in Stengel et al. (2018). The purpose of the SIMplistic cloud simulator For ERA-Interim (SIMFERA) developed in the framework of ESA Cloud_cci is to evaluate the cloud parameterization used in ECMWF models, although SIMFERA is assumed to be applicable to other model data too. In general SIMFERA consists of three modules: (1) downscaler, which converts the model grid box mean profiles into sub-grid profiles considering the mismatch in spatial scale between that of a model and that of a satellite pixel; (2) pseudoretrieval, which emulates the pixel-scale cloud parameters based on the sub-grid profiles; and (3) statistical aggregation, which builds the diagnostic output that is comparable to the observational dataset (i.e. temporal averages and histograms, see below).

The general features are:

- SIMFERA uses the three-dimensional (3D) model fields as input (see details below). The simplistic approach in offline mode has the advantage of short computation time (e.g. 33 years of reanalysis data processed in less than 2 days on a HPC system).
- Unlike sophisticated simulators, which are using modelled radiances and brightness temperatures to retrieve cloud optical parameters based on radiative transfer calculations (e.g., COT and CER following Nakajima-King method), SIMFERA stays very close to the original model fields. For instance, it uses the ERA-Interim CER parameterization (Martin et al. 1994, Sun and Rikus 1999, Sun 2001) along with the original 3D variables to convert the model state into comparable synthetic observations. Details are given in Stengel et al. (2017).
- No satellite overpass is taken into account as ERA-Interim is only available in discrete temporal resolution of several hours. However, day and night conditions are considered for the calculation of cloud optical parameters (i.e. COT, CER, CWP) that are only available during daytime observations since they are based on visible measurements.
- SIMFERA provides 2 options about how liquid and ice clouds occurring in the same model grid box are treated during the simulations (in the sub-column procedure): mixed phase (i.e. mixed phase clouds if both water/ice contents exists) or no-mixed phase (i.e. considering liquid and ice clouds separately).
- SIMFERA can be used for other model output evaluation after small modifications since there are not instrument/algorithm specifications implemented.

Input:

The simulator reads 6-hourly (00, 06, 12, 18 UTC) gridded estimates of 3D meteorological upper air parameters on 60 model levels including the following profiles: liquid water content "LWC" [kg/kg], ice water content "IWC" [kg/kg], cloud cover "CC" (0-1), temperature "T" [K], and specific humidity "Q" [kg/kg].

Additionally, the ERA-Interim file comprises for each grid box two-dimensional (2D) arrays of surface geopotential "Z" $[m^2/s^2]$ an logarithm of surface pressure "LNSP" [Pa].

The latter two parameters are required for the computation of vertical pressure and geopotential profiles by using the provided "A" and "B" coefficients on model levels along with T and Q profiles.

Output:

Grid box monthly means are computed averaging first over all sub-columns per grid box and then averaging over all diagnostic time steps per month. Histograms are based on sub-column values because the downscaled results mimic the spatial resolution of a satellite footprint.



Doc:			Cloud_cci+	_D6.2_FINAL_REPORT_Phase1_v1.0.docx
Date:				23/01/2024
Issue:	1	Revision:	0	Page 17

SIMFERA provides the following monthly mean products: total, high-, mid-, and low-level CFC (0-1), CPH (0-1), LWP and IWP $[g/m^2]$, CTP [hPa], CTH [km], and CTT [K], COT and CER [micron] for liquid and ice phase, 2D joint cloud property histograms following the ISCCP classification relating the simulated height and optical thickness of the clouds, and 1D histograms for CTP, CTT, CWP, COT, and CER with the cloud phase as additional dimension.

3.1.2 Adaptation in Cloud_cci+ Phase I

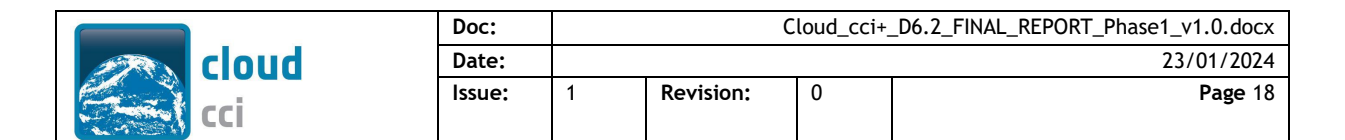
The following developments were done in Cloud_cci+ Phase I.

- Replacing ERA-Interim by ERA-5 as input, including increasing horizontal resolution from 1.0° to 0.5° and increasing the vertical resolution from 60 model levels to 137 model levels
 - Increasing number of sub-columns in the simulator from 20 to 40 (approx.. representing ~1km spatial resolution)
 - Applying SIMFERA to the entire year of 2019
- Aggregating to 0.5 L3C products (comparable to Cloud_cci+ SLSTR L3C)
- Porting the entire source code and processing environment to new ECMWF computer facilities (ATOS)

These tasks were not only done to update SIMFERA but also to adapt it to the SLSTR data processed in Cloud_cci+ Phase I. In the next section the results of a brief comparison between SIMFERA and SLSTR S3a data for 2019 are shown.

3.1.3 Summary of results

The SLSTR data referred to in this subsection are the Cloud_cci+ Phase I SLSTR S3a data version 3, for July 2019. Fehler! Verweisquelle konnte nicht gefunden werden. shows maps and zonal means of monthly mean cloud fraction from SLSTR and ERA-5 SIMFERA results, and the latter for three different COT thresholds. Generally ERA-5 shows good agreements with SLSTR between 60S and 60N with only small sensitivity to the applied COT threshold. In the high latitudesERA-5 has much more cloudiness than SLSTR when all clouds are considered. However, removing the thinnest clouds clearly increases the agreement in the Southern high latitudes. In the Northern high latitudes however, the ERA-5 cloud fraction shows only small change in these scenarios.



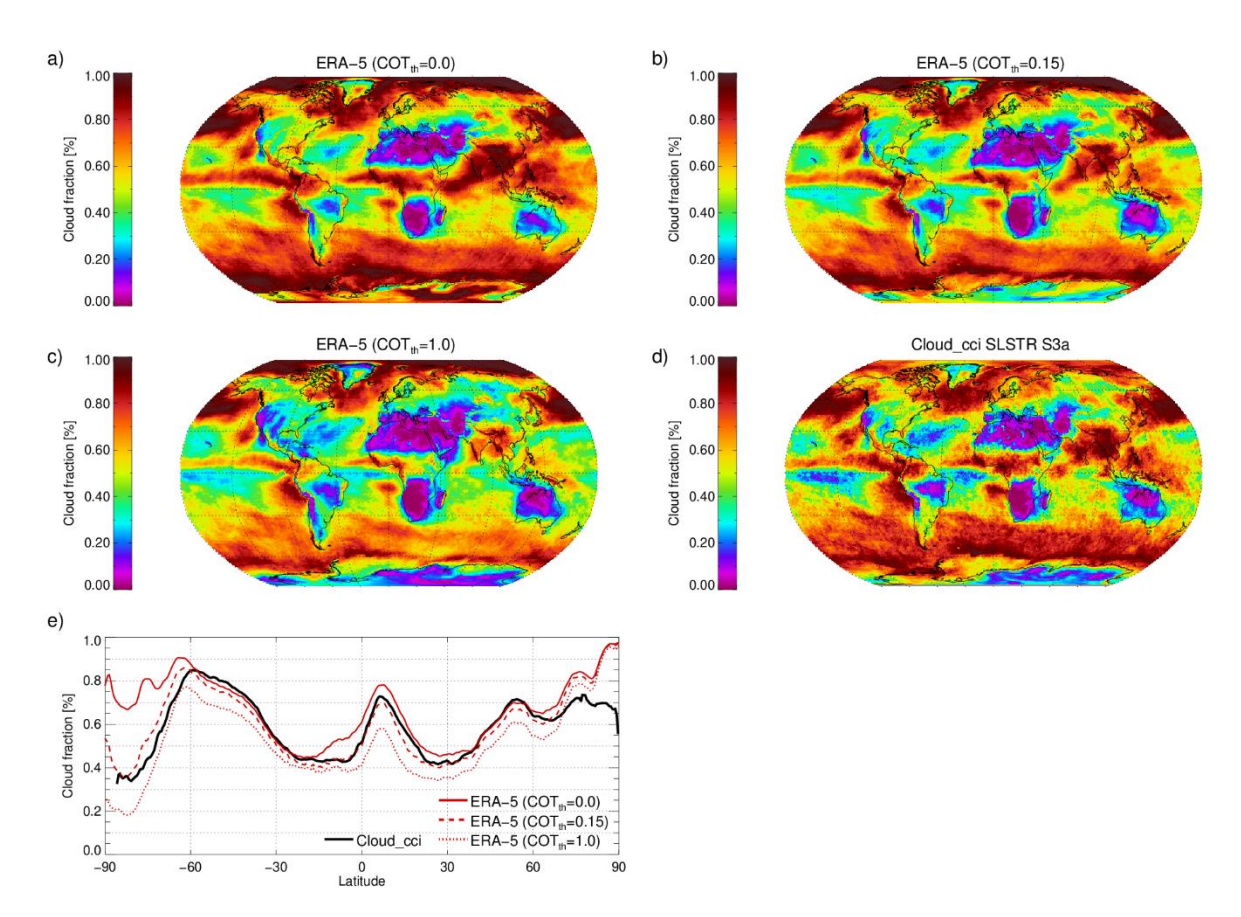


Figure 3-1 Monthly mean cloud fraction (CFC) from ERA-5 (a-c) and Cloud_cci+ v3 SLSTR S3a (d) for July 2019, where the ERA-5 cloud fraction was produced by SIMFERA for three optical thickness thresholds (COT_{th} = 0.0, 0.15, 1.0). Panel (e) is the zonal mean plot of CFC for all four sets. The uncertainty in Cloud_cci is mainly due to missing optically very thin clouds.

In Figure 3-2 the cloud fraction for low-, mid and high-level clouds are compared. The fraction of high-level clouds is much higher in ERA-5 than in SLSTR, which could point to a deficit in ERA-5 and/or to a lack of sensitivity to thin high-level clouds in SLSTR data. Removing cloud-top layers with an optical thickness below 1 brings the ERA-5 high-level cloud fraction down to SLSTR. For mid- and low-level clouds we generally see smaller values in ERA-5 compared to SLSTR, which is more pronounced for mid-level clouds.

Figure 3-3 depicts the relative frequency of cloud top pressure for SLSTR and ERA-5 stratified by cloud phase. While for liquid clouds the agreement between ERA-5 and SLSTR is reasonably (for all COT threshold), for ice clouds ERA-5 has clearly more high clouds (and less mid-level and low-level clouds) than SLSTR even when cloud top layers up to an optical thickness of 1 are removed from ERA-5. This confirms the findings for the cloud layer fractions above.

As last example, Figure 3-4 shows maps and zonal mean plots of monthly mean liquid cloud fraction. Between 50S and 50N the cloud phase agrees reasonably well, when no clouds layers are removed from ERA-5. Towards the higher latitudes, we find that ERA-5 has less liquid clouds than SLSTR, relatively speaking. Removing thin cloud top layers leads to generally increasing the liquid cloud fraction in ERA-5 by partly more than 20%.



Doc:			Cloud_cci+	_D6.2_FINAL_REPORT_Phase1_v1.0.docx
Date:				23/01/2024
Issue:	1	Revision:	0	Page 19

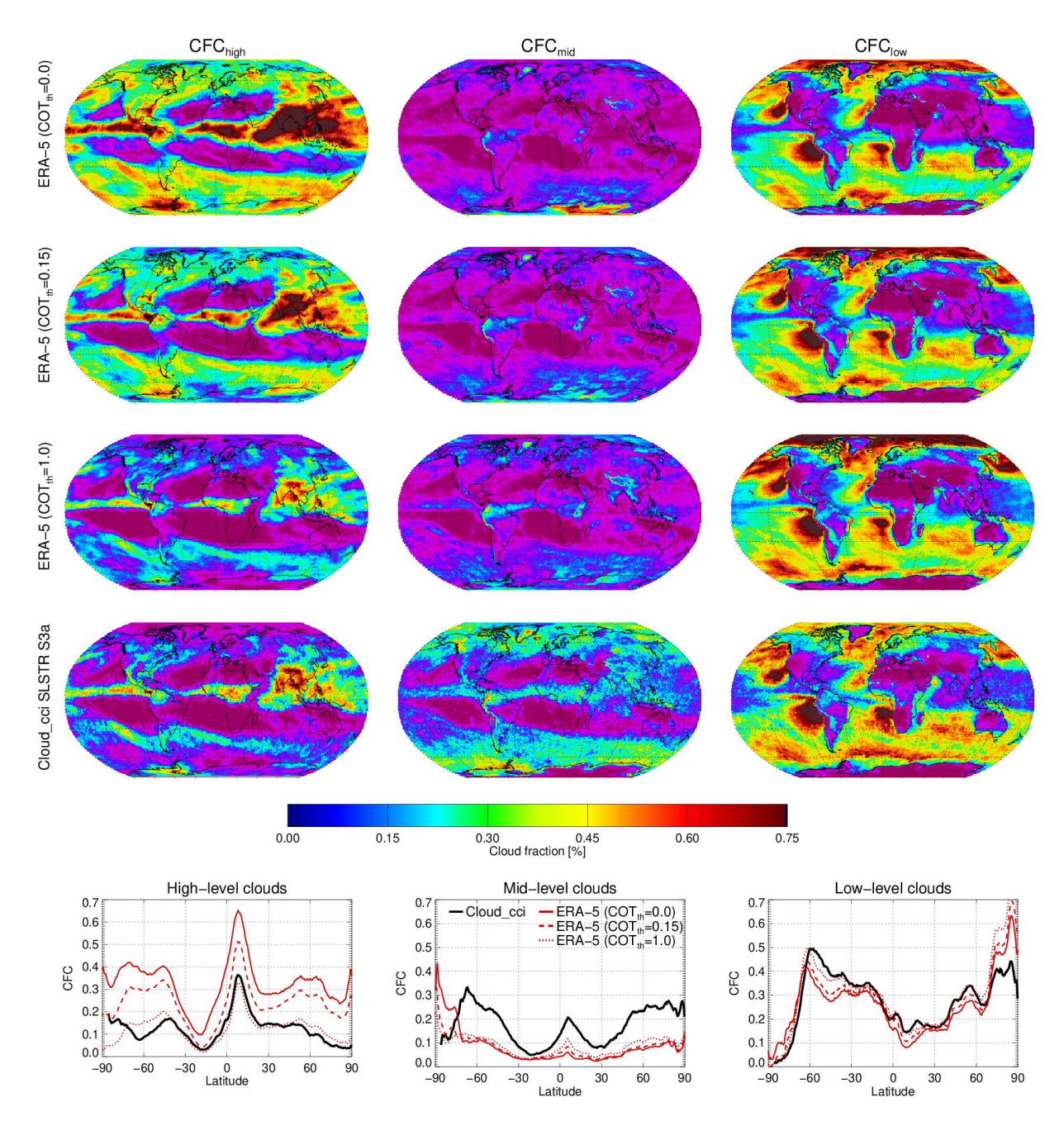
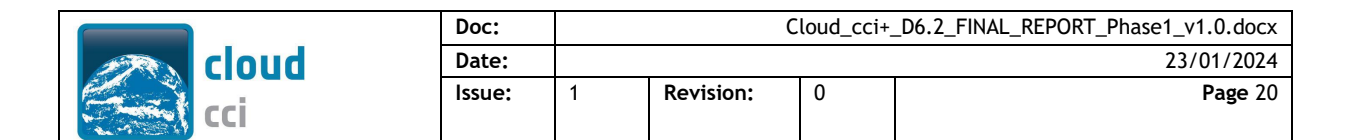


Figure 3-2 Monthly mean cloud fraction from ERA-5 (rows 1-3) and Cloud_cci+ v3 SLSTR S3a (row 4) for high-level (CFC_{high}, left column), mid-level (CFC_{mid}, middle column) and low-level clouds (CFC_{low}, right column) for July 2019. The ERA-5 cloud fraction was produced by SIMFERA for three optical thickness thresholds (COT_{th} = 0.0, 0.15, 1.0; rows 1 to 3, respectively). Bottom row: zonal mean plots for CFC_{high}, CFC_{mid} and CFC_{low}.



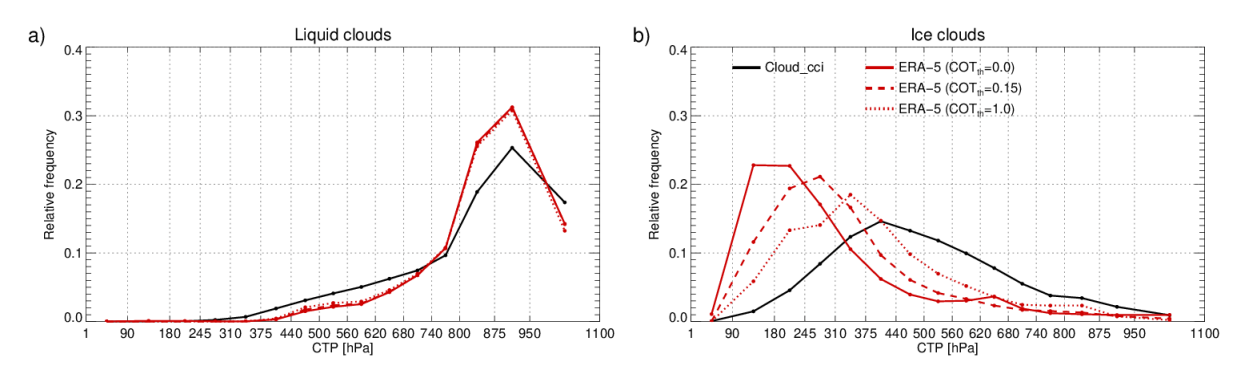


Figure 3-3 Global, relative frequency histograms of observed Cloud_cci cloud-top pressure (CTP) compared to ERA-5 CTP after applying SIMFERA with three COT thresholds COT_{th} (0.0, 0.15 and 1.00) - separated in liquid (a) and ice clouds (b) - for July 2019.

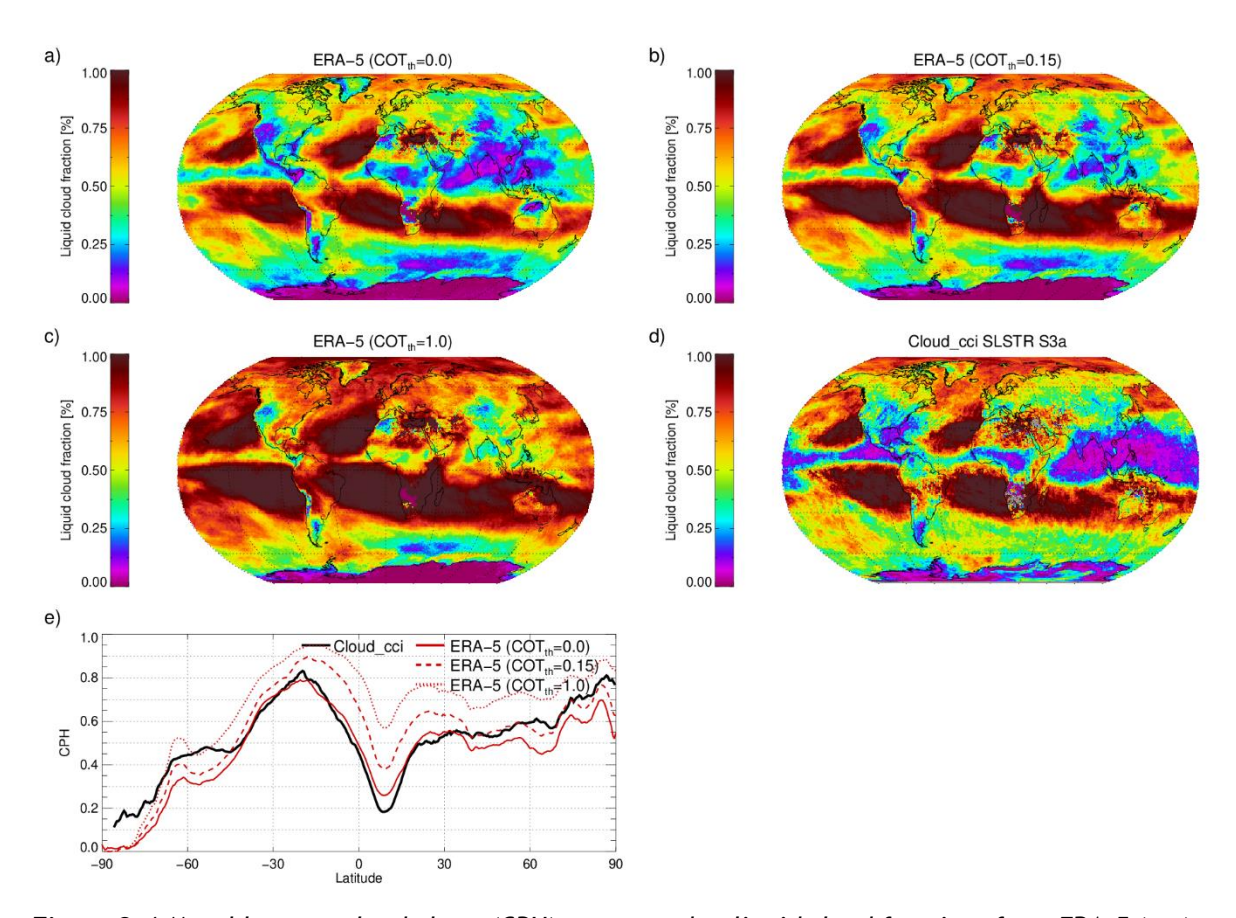
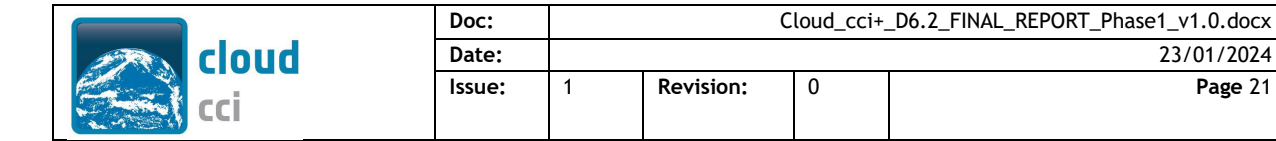


Figure 3-4 Monthly mean cloud phase (CPH), presented as liquid cloud fraction, from ERA-5 (a-c) and Cloud_cci+ v3 SLSTR S3a (d), where the ERA-5 liquid cloud fraction was produced by SIMFERA for three top-down optical thickness thresholds (COT_{th} = 0.0, 0.15, 1.0), at which the phase was collected from ERA-5 profiles. (e) Zonal mean plot of CPH for all four sets.



3.2 Uncertainty analysis & characterization

A set of work packages assessed the errors introduced into the Cloud_cci products by uncertainties in the ancillary data, or more specifically, in variables which are used but are not part of the state vector: surface emissivity, temperature profiles and specific humidity profiles. Furthermore, the uncertainties in monthly mean cloud products introduced by the incomplete diurnal sampling of polarorbiting sensors (e.g. SLSTR, AVHRR) are assessed. Finally, SLSTR and SEVIRI data were compared to assess the impact of using different spectral information on the resulting cloud products. In the following subsections the total error budget for ancillary information is summarized as well as the results of the sampling uncertainty analysis shown. The reader is referred to E3UBv1 to access all results.

3.2.1 Error budget for ancillary information

Figure 3-5 shows the error budget for all ancillary error terms (S_{anc,e_s} , $S_{anc,T}$, $S_{anc,q}$ and S_{anc}) for each of the six ISCCP cloud types considered in the present work. For comparison, we have also plotted (black dots) uncertainties currently assumed for each thermal channel that account for non-ancillary parameter uncertainty, uncertainties associated with co-registration and scene homogeneity, and forward model uncertainty. The results of the error budget further reveal clear differences in the forward model uncertainty sensitivity between the optically thin and thick cloud types.

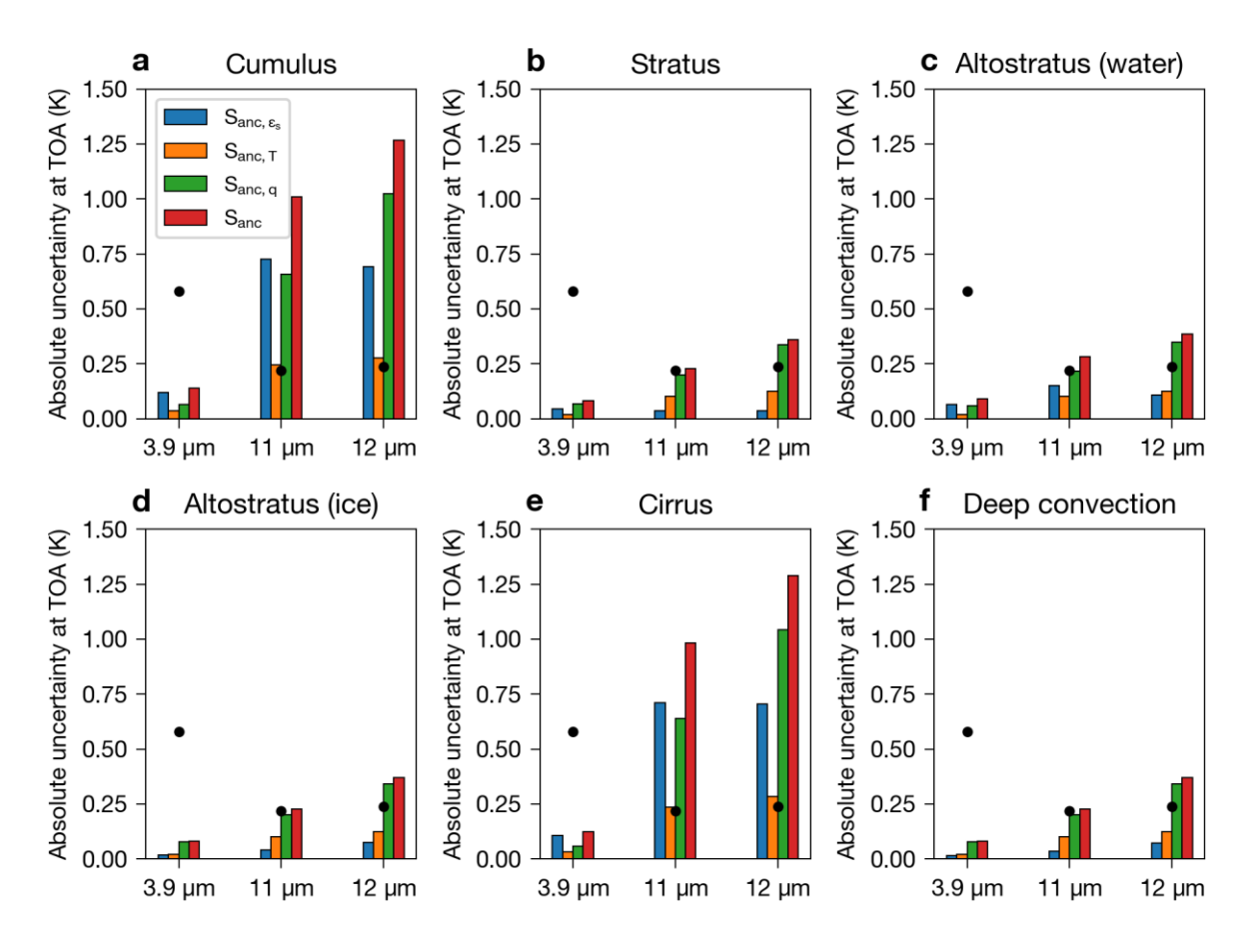


Figure 3-5 Error budget accounting for uncertainties in ancillary information for (a) Cumulus, (b) Stratus, (c) Altostratus in the liquid water phase, (d) Altostratus in the ice phase, (e) Cirrus and (f) Deep convection. See Table 1 for ISCCP cloud definitions. Note that the values shown represent the square root of the diagonal of the error covariance matrices. Black dots indicate currently assumed non-ancillary parameter uncertainty (in K).

23/01/2024

Page 21



Doc:			Cloud_cci+	_D6.2_FINAL_REPORT_Phase1_v1.0.docx
Date:				23/01/2024
Issue:	1	Revision:	0	Page 22

3.2.2 Sampling uncertainty

Temporally highly resolved, geostationary observations were utilized to analyse the potential systematic errors introduced by reduced, and thus potentially imperfect, diurnal sampling of polar-orbiting sensors (e.g. SLSTR). Figure 3-6 (morning orbits) and Figure 3-7 (afternoon orbits) show frequency distributions over the mean differences for all main cloud variables for varying sampling scenarios (observations times). Relatively speaking, the reduced temporal sampling — twice per day for CFC, CTP and CPH and once per day for COT, LWP and IWP — does not introduce severe systematic uncertainties when considered over a larger domain. Furthermore, the biases remain small as observation time is varied. For CFC the bias is most positive around midday. CTP and CPH show a similarly less negative / more positive at midday compared to morning and afternoon. The bias for COT remains relatively small throughout the day, with a decrease around midday. For LWP, the bias becomes more negative through the day, while the opposite is observed for IWP. A slight exception is CTP, for which an increasingly positive bias is seen towards midday, decreasing thereafter.

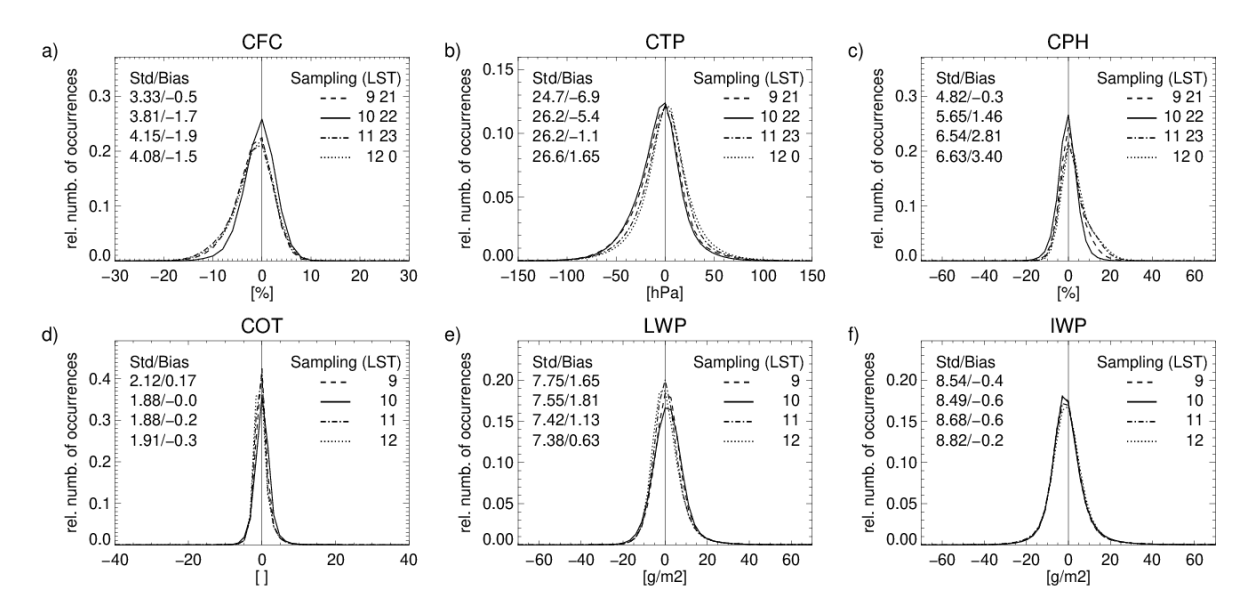
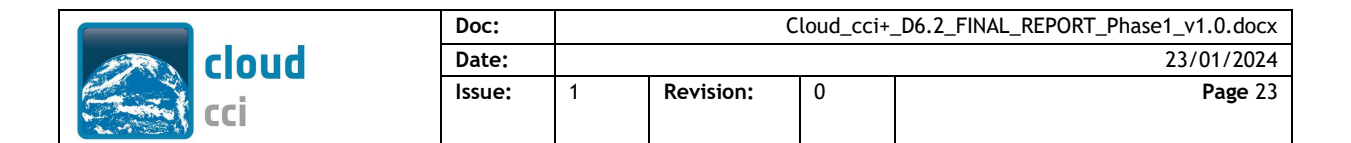


Figure 3-6 Sampling uncertainty for polar-orbiting sensors for morning overpasses at 9:00, 10:00, 11:00, 12:00 local solar time. Statistics are derived from temporally subsampling geostationary (SEVIRI) 15min data. For CFC, CTP and CPH the sampling is done twice as day (ascending and descending node), while for COT, LWP and IWP the data shown only including daylight overpasses.

This analysis also enables a basic quantification of theoretical trends in the any time series analysis caused by orbital drift, i.e. when the orbit and thus the local observation times do not remain stable over time:

- 1. Assuming an overpass time of 10:00 and a drift of the overpass time to 11:00 within 5 years, the 5-year trends introduced by this drift amount to: -0.2% for CFC, +4.3 hPa for CTP, +1.35% for liquid cloud fraction (CPH), -0.2 for COT, -0.68 g/m-2 for LWP and 0 g/m-2 for IWP.
- 2. Assuming an overpass time of 14:00 and a drift of the overpass time to 15:00 within 5 years, the 5-year trends introduced by this drift amount to: +0.9% for CFC, -1.7 hPa for CTP, -1.64% for liquid cloud fraction (CPH), +0.1 for COT, -1.08 g/m-2 for LWP and +0.77 g/m-2 for IWP.



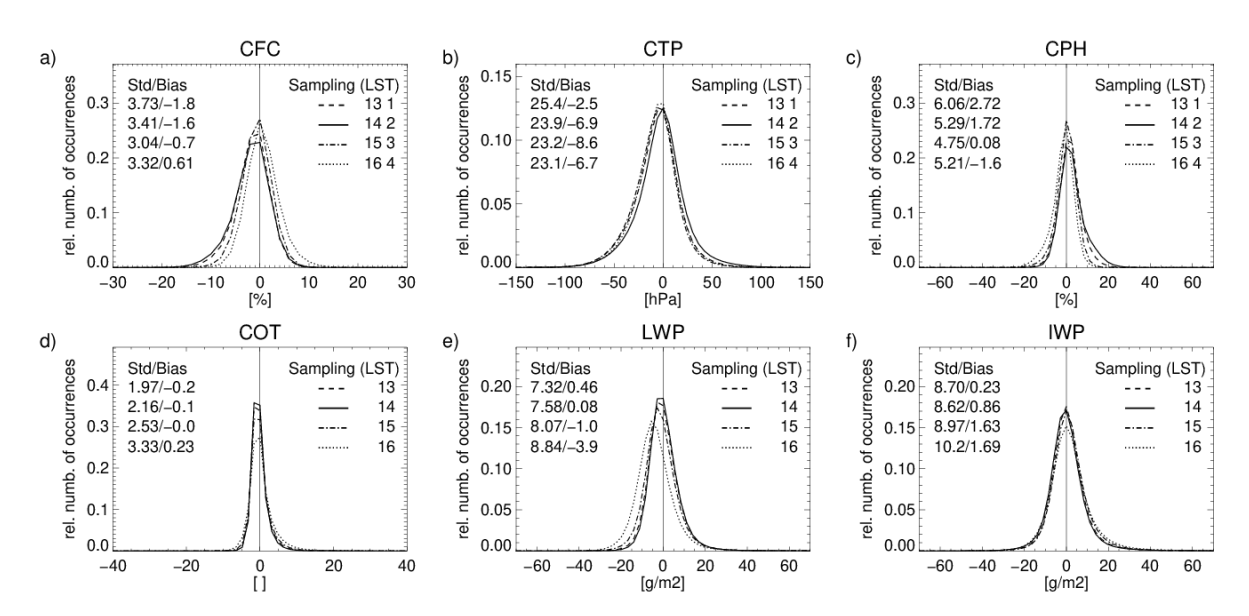


Figure 3-7 As Figure 3-6 but for the afternoon overpass times 13:0, 14:00, 15:00 and 16:00.



Doc:			Cloud_cci+	_D6.2_FINAL_REPORT_Phase1_v1.0.docx
Date:				23/01/2024
Issue:	1	Revision:	0	Page 24

4 User Case Studies

4.1 User Case Study I - A Lagrangian Perspective on the Lifecycle and Cloud Radiative Effect of Deep Convective Clouds Over Africa

The report in this section is a brief summary of Jones et al. (2023) with most parts (text and figures) being copied-pasted from the manuscript.

4.1.1 Scope

In this study cloud and radiative flux properties from the Cloud_cci+ SEVIRI dataset was utilized. In a 4 month period, deep convective systems (DCCs) are identified, tracked and their life cycle investigated with respect to the top-of-atmosphere cloud radiative effect of their anvil clouds. Their cumulative effects are analysed and put in relation of the (a) initiation time of the DCCs, (b) their lifetime, and (c) the number of core a DCC has.

4.1.2 Summary

Figure 4-1 shows the frequency of detected convective cores. Figure 4-2 shows the net cloud radiative effect and its components for three selected cases:

- a) A rather short-lived DCC which is initiated in the afternoon and which dissipates in the early evening. This DCC has a negative cumulative radiative effect (cooling)
- b) A DCC that exists almost 24 hours into the morning of the next day. This DCC has a positive cloud radiative effect (warming)
- c) A clustered DCC that had multiple cores and lived several days. The cumulative cloud radiative effect of this system is very close to zero.

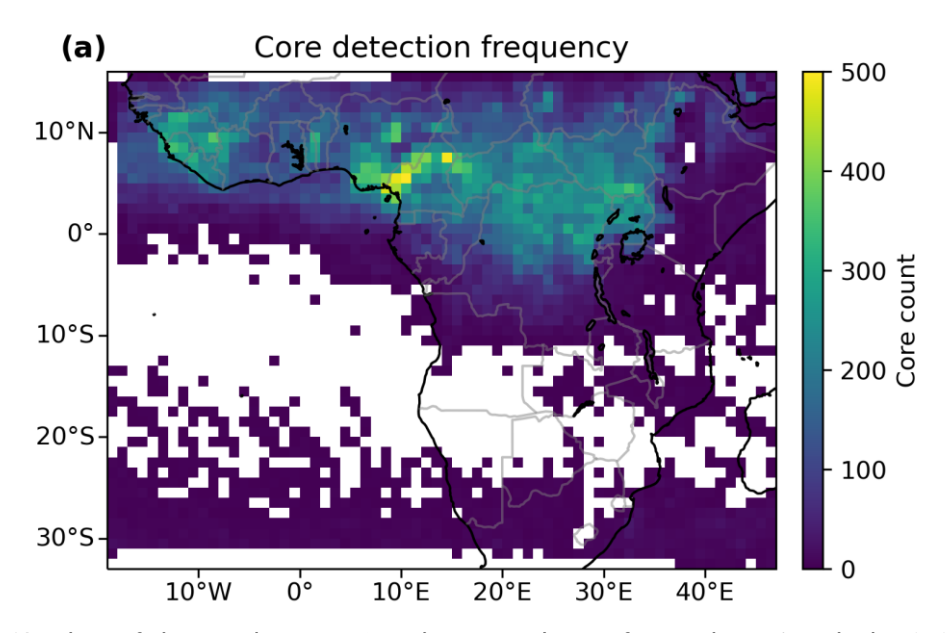
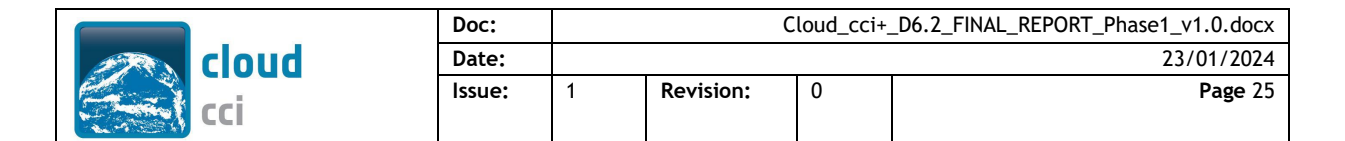


Figure 4-1 Number of detected cores (a) and average hour of core detection (b) by 1x1° grid box. Grid boxes in (b) with a standard deviation greater than 6 hours are single-hatched, and greater than 12 hours cross-hatched. Figure and caption taken from **Jones et al.** (2023).

Figure 4-3 shows the histogram over the mean cloud radiative effect of all track DCCs in the 4 month period. It depicts that there is a bimodal distribution with the first mode peaking around -200 Wm⁻² (cooling) composed of the short-lived single-core DCCs. The second mode peaking around 100 Wm⁻² (warming) is composed of the longer-living DCCs. However, the mean cloud radiative of the clustered



multi-core DCC is around 0 Wm^{-2.} And interestingly, the mean cloud radiative effects over all DCCs is also close to zero, despite the two modes. The later confirms the common assumption that Tropical DCCs have a nearly neutral effects on the top of atmosphere radiative budget.

More information on this study can be found in Jones et al. (2023).

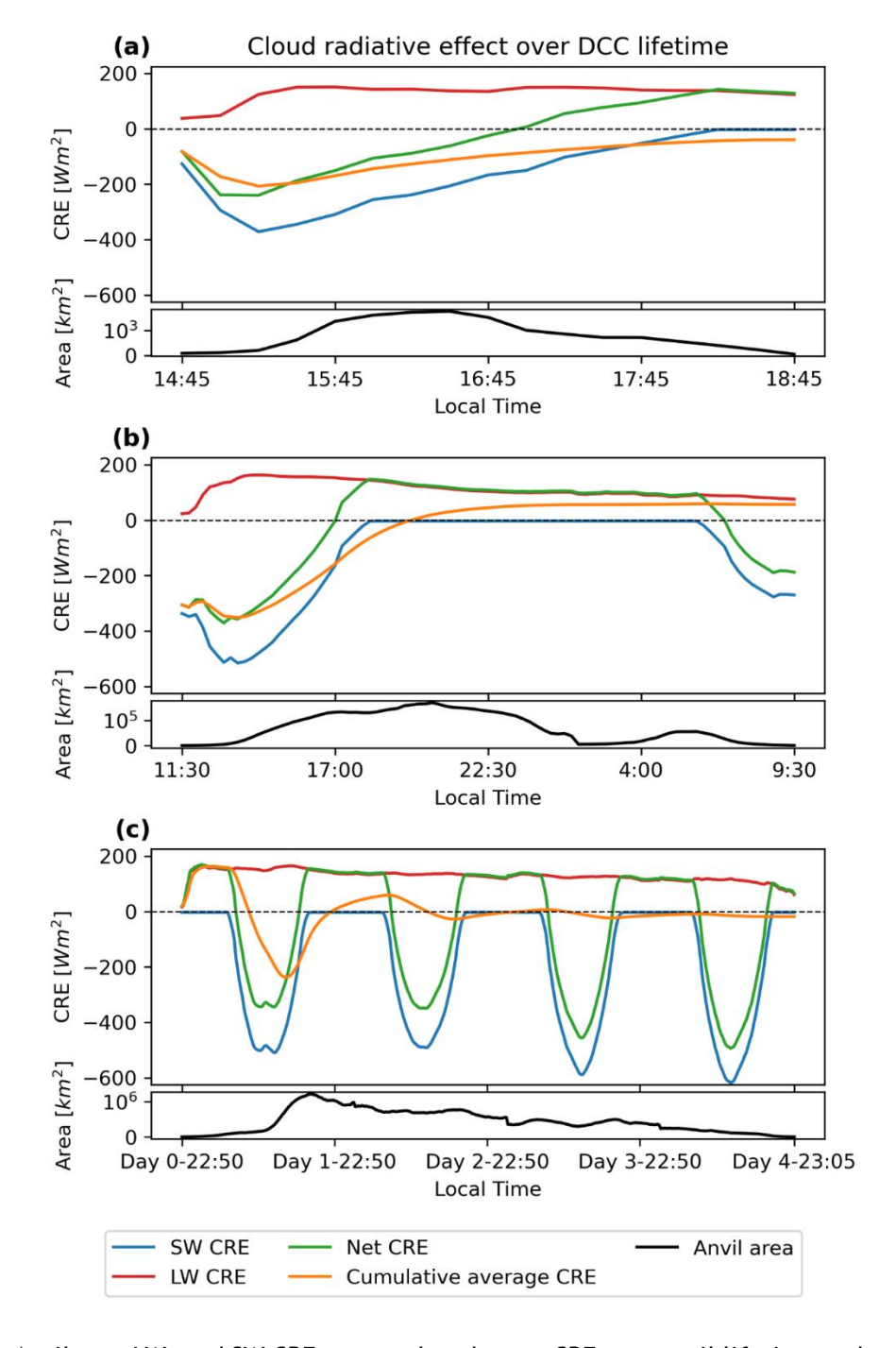


Figure 4-2 Anvil net, LW, and SW CRE, accumulated mean CRE over anvil lifetime and anvil area for (a) an isolated, short-lived (4-hour) DCC, (b)a moderately clustered, 1-day long DCC, and (c) a large, clustered, 4-day long DCC. All times are the local solar time, to the nearest 5 minute interval. Figure and caption taken from **Jones et al. (2023)**.



Doc:			Cloud_cci+	_D6.2_FINAL_REPORT_Phase1_v1.0.docx
Date:				23/01/2024
Issue:	1	Revision:	0	Page 26

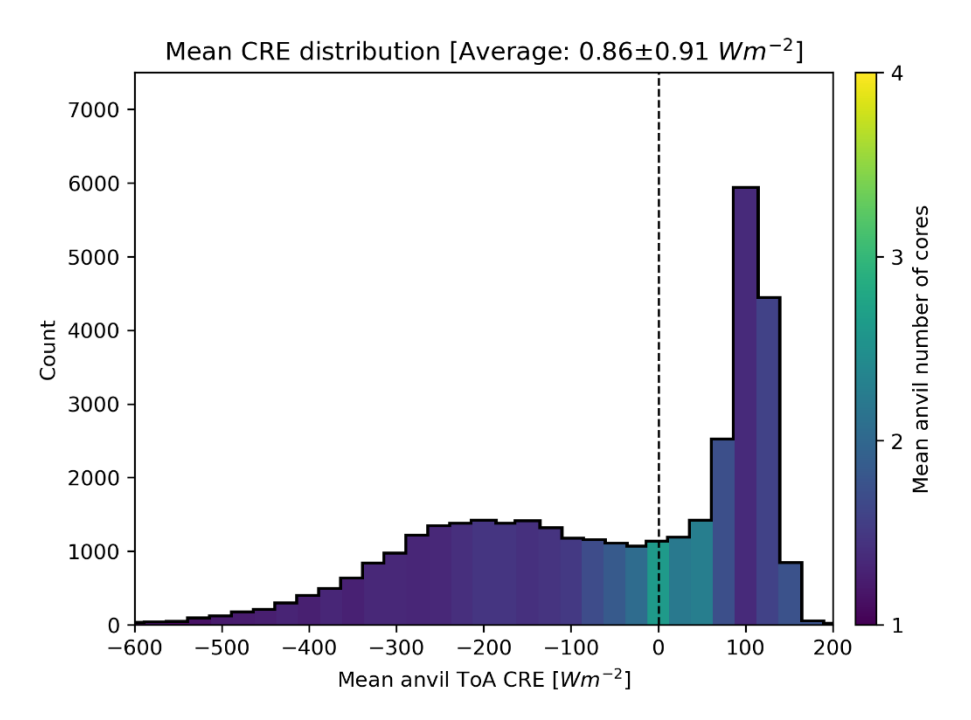


Figure 4-3 The distribution of lifetime anvil CRE for all observed anvils. The mean number of cores per anvil in each bin is indicated by the colour scale. The vertical dashed line shows the integrated mean CRE over all anvils, weighted by the anvil areas $(0.86\pm0.91~\mathrm{Wm^{-2}})$. Figure and caption taken from **Jones et al.** (2023).

4.2 User Case Study II - Designing a 'Sunny Vacation Map' based on Satellite Observations on Clouds and Radiation

The report in this section is a summary of RUCS2.

4.2.1 Scope

This study highlights a specific aspect of how long-term satellite observations of cloud and radiation properties facilitate real-life applications. Having more than three decades of those observations available provides a very sound basis for a statistical analysis of not only the occurrence of sunny days (more or less the inverse of cloud fraction), but also how these are clustered.

In this report the determination of sunny days is described and how sunny periods are defined as function of the sunny day sequences. Global maps of the likelihood of sunny periods are shown, stratified by season, and discussed.

In addition, two pairs of European cities were selected to compare the general likelihood of sunny periods and elaborate on the temporal evolution of this information throughout the whole time series.

This study is considered as teaser for a potential operational application.

4.2.2 Data basis

Basis of our analysis is the Cloud_cci AVHRR-PMv3 dataset (Stengel et al., 2020), compiled within ESA's Cloud Climate Change Initiative (Cloud_cci) Phase 2. It is a global dataset on clouds and



Doc: Clo	Juu_cci+_	_D6.2_FINAL_REPORT_Phase1_v1.0.docx
Date:		23/01/2024
Issue: 1 Revision:	0	Page 27

radiation covering the period of 1982 to 2016, which results in a long-term data record of 35 years - long enough to consider it a climatology.

Cloud and radiation properties were retrieved from passive remote sensing measurements recorded by the Advanced Very High Resolution Radiometer (AVHRR) - in particular by those flying on afternoon (PM) polar orbiting satellites of the National Oceanic and Atmospheric Administration (NOAA). They encircle the Earth from pole to pole about a dozen times per day, gathering information from all around the globe. PM satellites are those satellites that have an equator crossing time in the afternoon (local solar time). See Fehler! Verweisquelle konnte nicht gefunden werden. for an overview of all satellites included and their respective equator crossing times.

4.2.3 Approach

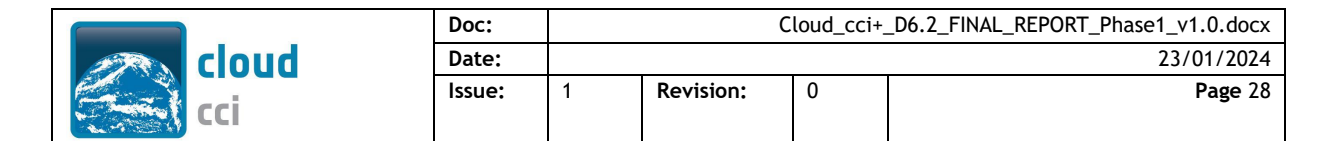
The likelihood of a sunny period is here defined as the probability to get at least "x" days of sunshine within a total amount of "n" days of vacation, which might be one of the most valuable information for a holiday maker.

Sunny days are days for which the ratio of obtained to possible shortwave radiation being bigger than 0.85 (and for "cloudy" being smaller than 0.85).

4.2.4 Summary of results

As an example result, Figure 4-4 illustrates the results of our global analysis, the global "sunny vacation map" of sunny periods: It gives the likelihood to get at least 5 sunny days within 7 days of vacation lying ahead, spatially resolved on global scale (albeit slightly coarser than possible, see above) and depending on the time of the year. Oceanic regions are masked out as the typical holiday resort is on land, unless it is a sailing trip or cruise. The map reveals that, globally seen, the whole range of possible probabilities for sunny periods is covered, ranging from nearly 0% in e.g. the inner tropics near the equator to almost 100% in desert regions like the Sahara. Primarily, the probability for sunny periods varies with latitude. It is generally large (more than 60% in the mean) in the subtropics, where large-scale subsidence typically supresses the formation of clouds. It is rather small (less than 20% in the mean) in the outer tropics, where strong insolation triggers intense cloud formation. And it is moderate (between 10 to 40%) in the mid-latitudes, where highs and lows frequently alternate, usually bringing a diverse mix of sun and clouds.

More information on this User Case Study can be found in RUCS2.



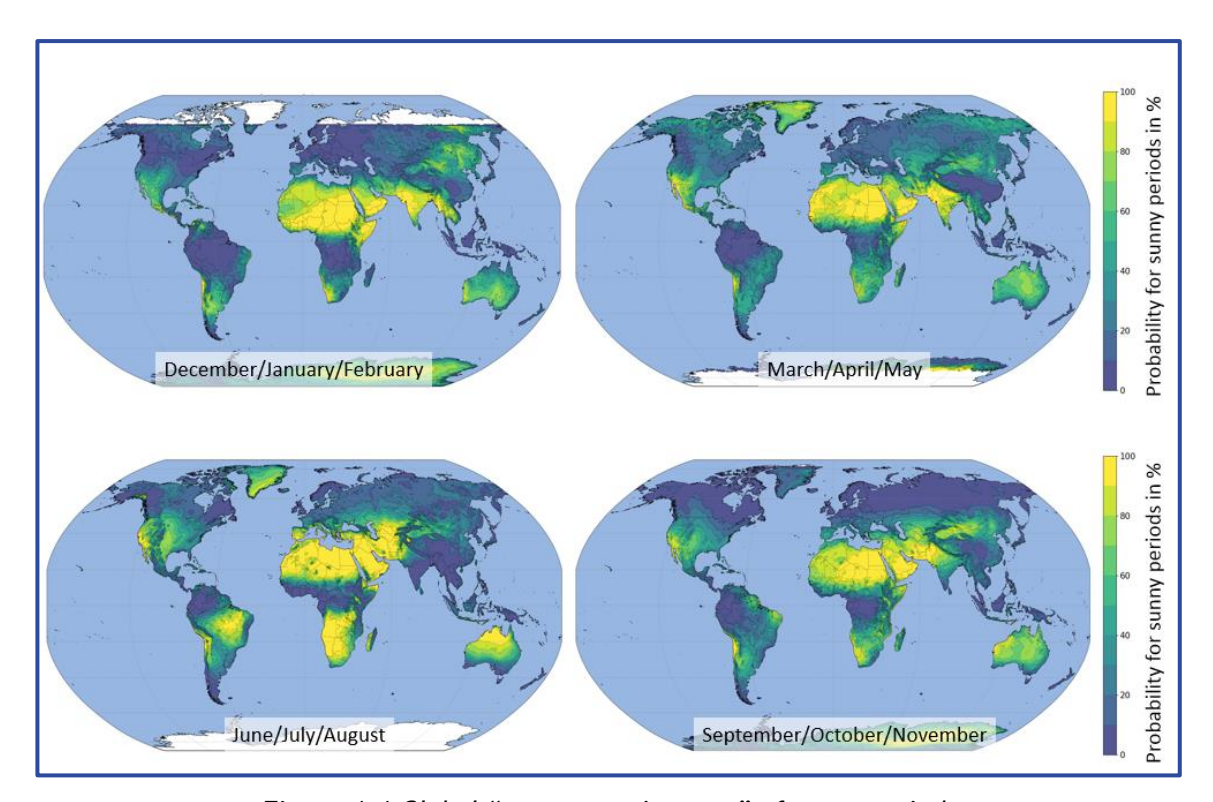


Figure 4-4 Global "sunny vacation map" of sunny periods

4.3 Singular Vector Decomposition (SVD) of satellite datasets: relation between cloud properties and climate indices

The report in this section is a brief summary of Carboni et al. (2023) with most parts (text and figures) being copied-pasted from the manuscript.

4.3.1 Scope

We describe a technique using singular vector decomposition (SVD) to identify the spatial patterns that best describe the temporal variability of a global satellite dataset. These patterns, and their temporal evolution, are then correlated with established climate indices. We apply this technique to datasets of cloud properties over three decades derived from five visible/IR imagers (ATSR-2, AATSR, SLSTR-A & -B and MODIS) and from the IR and microwave sounders on MetOp (IASI, MHS, AMSU-A). However, it could potentially be used more generically to extract the pattern of variability of any regular gridded dataset from satellites or models. Figure 4-5 shows the monthly mean cloud fraction (CFC) and cloud top height (CTH) for the three datasets considered for the month of February 2019. All three datasets have global coverage and show similar spatial patterns 65 of CFC and CTH, but there is some disagreement in the magnitude. The IMS data in particular presents lower CFC and higher CTH compared to the other two datasets.

4.3.2 Method

- · Monthly-mean de-seasonalized anomaly for cloud fraction & cloud-top height:
 - For each instrument record, the multi-year mean for each month is subtracted
 - Accounts for inter-instrument offsets though precludes trend detection over the full multi-instrument record from ATSR-2/AATSR/SLSTR-A/SLSTR-B for 1996-2012.
- Singular Vector Decomposition (SVD):
 - SVD is a mathematical technique used to decompose a matrix of data into a set of

	Doc:		C	loud_cci+	_D6.2_FINAL_REPORT_Phase1_v1.0.docx
cloud	Date:				23/01/2024
cci	Issue:	1	Revision:	0	Page 29

orthogonal singular vectors and their temporal weights, which can enable patterns and trends in the dataset to be identified.

- Singular vectors here are the spatial patterns of de-seasonalised anomaly time series.
- The temporal weights of the SVs enable variability in the de-seasonalised anomaly time series to be re-constructed.
- · Climate indices (from NOAA) are fitted to temporal weights of leading singular vectors
 - Up to three climate indices are included in each fit with lags of up to ± 6mths

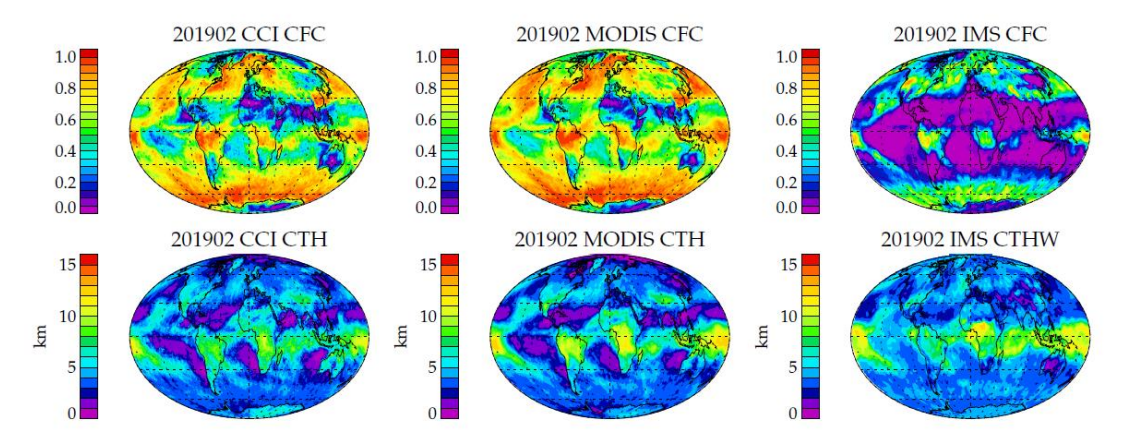


Figure 4-5 Monthly mean cloud fraction (CFC) and cloud top high (CTH), for the month of February 2019, from the tree datasets considered: (i) (A)ATSR and SLSTR data from Cloud_cci and Copernicus Climate Change Service (C3S); (ii) MODIS NASA; (iii) MetOp/IMS. Figure and caption taken from Carboni et al. (2023)

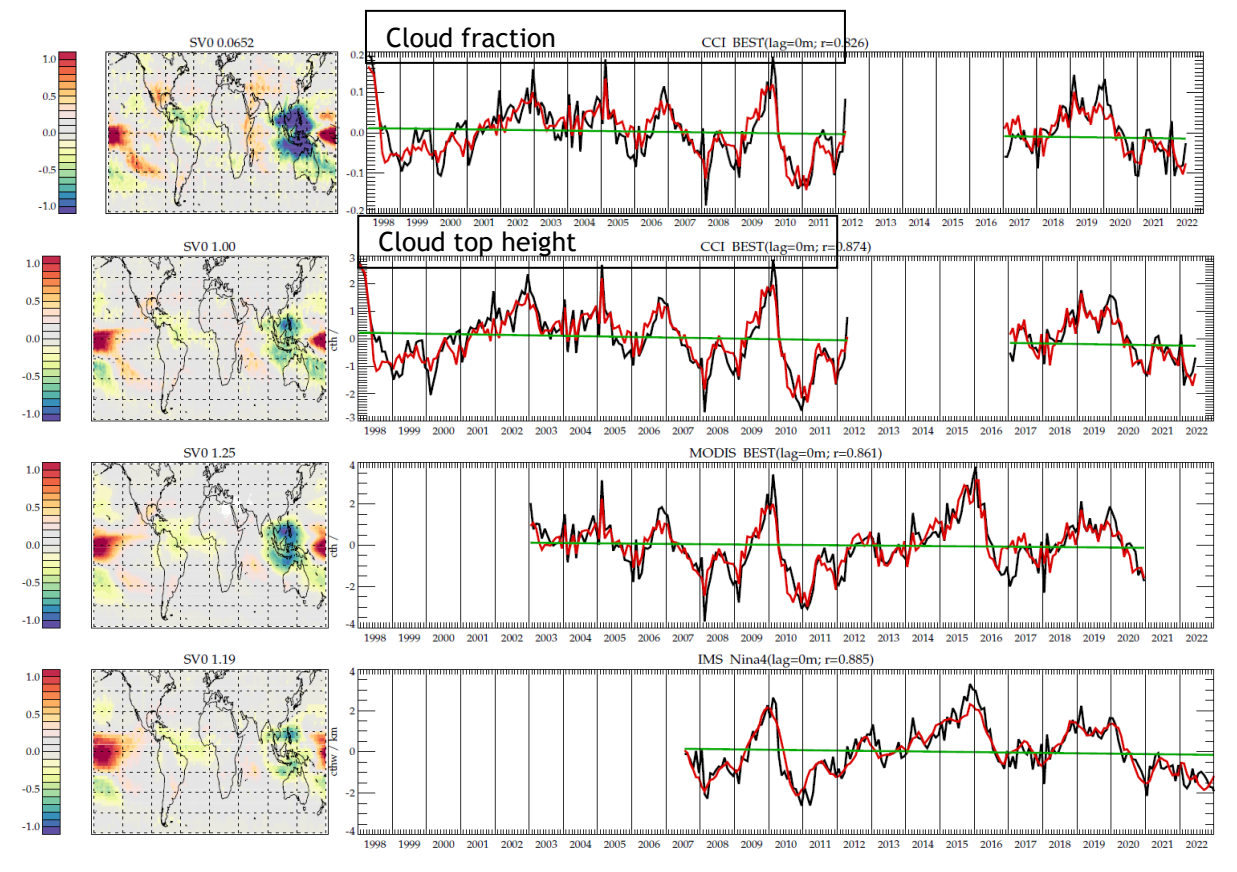


Figure 4-6 Maps of each leading SV and line plots of time series of their associated temporal weights (black) and fitted climate index (red). Legend above each time-series panel indicates satellite data



Doc:		(Cloud_cci+	_D6.2_FINAL_REPORT_Phase1_v1.0.docx
Date:				23/01/2024
Issue:	1	Revision:	0	Page 30

set, fitted climate index, lag and correlation coefficient (r). Strong correlation with zero lag is seen between the leading SV and ENSO index "BEST" or "Nina4" in all four cases. Figure and caption taken from Carboni et al. (2023)

4.3.3 Conclusions

- SVD of de-seasonalised monthly anomalies has enabled a new approach to compare the satellite data on cloud over three decades with climate indices
- Leading SV for three independent global data sets on both cloud fraction and cloud-top height from polar orbiting satellites covering different time periods is strongly correlated with ENSO indices.
- The SVD approach could potentially offer a new tool for using global satellite observations to assess global climate model (GCM) or Earth System Model performance.

More information on this study can be found in Carboni et al. (2023).



Doc:			Cloud_cci+	_D6.2_FINAL_REPORT_Phase1_v1.0.docx
Date:				23/01/2024
Issue:	1	Revision:	0	Page 31

5 References

ADPv3.0, 2023: ESA Cloud_cci+ Algorithm Development Plan (ADP), Issue: 3 Revision: 0, Date of issue: TBD, TBD, Available at https://climate.esa.int/en/projects/cloud/

ATBDv9.0, 2022, ESA Cloud_cci+ Algorithm Theoretical Baseline Document (ATBD), Issue 9, Revision: 0, Date of Issue: TBD, Available at https://climate.esa.int/en/projects/cloud/

ATBD-CC4CLv9, Algorithm Theoretical Baseline Document (ATBD) CC4CL - ESA Cloud_cci, Issue 5, Revision: 0, date of Issue: : TBD, Available at: https://climate.esa.int/en/projects/cloud/key-documents/

ATBD-CC4CL_TOA_FLUXv1.1, Algorithm Theoretical Basis Document (ATBD) of the Community Code for CLimate (CC4CL) Broadband Radiative Flux Retrieval (CC4CL-TOAFLUX) - ESA Cloud_cci, Issue 1, Revision: 1, date of Issue: 14/10/2019, Available at: https://climate.esa.int/en/projects/cloud/key-documents/

Carboni, E., Thomas, G. E., Siddans, R., and Kerridge, B.: Singular Vector Decomposition (SVD) of satellite datasets: relation between cloud properties and climate indices, Atmos. Meas. Tech. Discuss. [preprint], https://doi.org/10.5194/amt-2023-232, in review, 2023.

CRDPv3, 2023: ESA Cloud_cci+ Climate Research Data Package (CRDP): Issue 3 Revision 0, Date of issue: TBD, Available at https://climate.esa.int/en/projects/cloud/

E3UBv1, 2023: ESA Cloud_cci+ End to End ECV Uncertainty Budget (E3UB): Issue 1 Revision 0, Date of issue: TBD, Available at https://climate.esa.int/en/projects/cloud/

Jones W. K., Stengel, M., and Stier, P.: A Lagrangian Perspective on the Lifecycle and Cloud Radiative Effect of Deep Convective Clouds Over Africa, EGUsphere [preprint], https://doi.org/10.5194/egusphere-2023-2059, 2023.

McGarragh, G. R., Poulsen, C. A., Thomas, G. E., Povey, A. C., Sus, O., Stapelberg, S., Schlundt, C., Proud, S., Christensen, M. W., Stengel, M., Hollmann, R., and Grainger, R. G.: The Community Cloud retrieval for CLimate (CC4CL) - Part 2: The optimal estimation approach, Atmos. Meas. Tech., 11, 3397-3431, https://doi.org/10.5194/amt-11-3397-2018, 2018.

PVIRv2.0, Product Validation and Intercomparison Report (PVIR) - ESA Cloud_cci+, Issue 2, Revision: 0, Date of Issue: 24/11/2022 Available at: https://climate.esa.int/en/projects/cloud/key-documents/

PVIRv3.0, Product Validation and Intercomparison Report (PVIR) - ESA Cloud_cci+, Issue 3, Revision: 0, Date of Issue: 10/07/2023 Available at: https://climate.esa.int/en/projects/cloud/key-documents/

Rossow, William B., and Robert A. Schiffer. "Advances in understanding clouds from ISCCP." Bulletin of the American Meteorological Society 80, no. 11 (1999): 2261.

RUCS2, **2020**: ESA Cloud_cci+ Report on User Case Study 2: Designing a "Sunny Vacation Map" based on Satellite Observations on Clouds and Radiation, Issue: Issue 1 Revision 0, Released: 17.03.2021, Available at https://climate.esa.int/en/projects/cloud/

PUGv1, 2023, ESA Cloud_cci+ Product User Guide (PUG), Issue 1, Revision: 1, date of Issue: TBD, Available at https://climate.esa.int/en/projects/cloud/

SSD, **2022**: ESA Cloud_cci+ System Specification Document, Issue: 5 Revision 0, Released: 25.07.2022, Available at https://climate.esa.int/en/projects/cloud/

Stengel, M., Stapelberg, S., Sus, O., Schlundt, C., Poulsen, C., Thomas, G., Christensen, M., Carbajal Henken, C., Preusker, R., Fischer, J., Devasthale, A., Willén, U., Karlsson, K.-G., McGarragh, G. R., Proud, S., Povey, A. C., Grainger, R. G., Meirink, J. F., Feofilov, A., Bennartz, R., Bojanowski, J. S.,



Doc:			Cloud_cci+	_D6.2_FINAL_REPORT_Phase1_v1.0.docx
Date:				23/01/2024
Issue:	1	Revision:	0	Page 32

and Hollmann, R.: Cloud property datasets retrieved from AVHRR, MODIS, AATSR and MERIS in the framework of the Cloud_cci project, Earth Syst. Sci. Data, 9, 881-904, https://doi.org/10.5194/essd-9-881-2017, 2017.

Stengel, M., Schlundt, C., Stapelberg, S., Sus, O., Eliasson, S., Willén, U., and Meirink, J. F.: Comparing ERA-Interim clouds with satellite observations using a simplified satellite simulator, Atmos. Chem. Phys., 18, 17601-17614, https://doi.org/10.5194/acp-18-17601-2018, **2018**.

Stengel, M., Stapelberg, S., Sus, O., Finkensieper, S., Würzler, B., Philipp, D., Hollmann, R., Poulsen, C., Christensen, M., and McGarragh, G.: Cloud_cci Advanced Very High Resolution Radiometer post meridiem (AVHRR-PM) dataset version 3: 35-year climatology of global cloud and radiation properties, Earth Syst. Sci. Data, 12, 41-60, https://doi.org/10.5194/essd-12-41-2020, **2020**.

Stengel, M., Meirink, J. F., & Eliasson, S. (2023). On the temperature dependence of the cloud ice particle effective radius—A satellite perspective. Geophysical Research Letters, 50, e2022GL102521. https://doi.org/10.1029/2022GL102521

Sun, Z. (2001). Reply to comments by Greg M. McFarquhar on "Parametrization of effective sizes of cirrus-cloud particles and its verification against observations." (October B, 1999,125, 3037 3055). Quarterly Journal of the Royal Meteorological Society, 127(571), 267-271. https://doi.org/10.1002/qj.49712757116

Sun, Z., & Rikus, L. (1999). Parametrization of effective sizes of cirrus-cloud particles and its verification against observations. Quarterly Journal of the Royal Meteorological Society, 125(560), 3037-3055. https://doi.org/10.1002/qj.49712556012

Sus, O., Stengel, M., Stapelberg, S., McGarragh, G., Poulsen, C., Povey, A. C., Schlundt, C., Thomas, G., Christensen, M., Proud, S., Jerg, M., Grainger, R., and Hollmann, R.: The Community Cloud retrieval for CLimate (CC4CL) - Part 1: A framework applied to multiple satellite imaging sensors, Atmos. Meas. Tech., 11, 3373-3396, https://doi.org/10.5194/amt-11-3373-2018, 2018.



Doc:		Cloud_cci+_D6.2_FINAL_REPORT_Phase1_v1.0.docx		
Date:				23/01/2024
Issue:	1	Revision:	0	Page 33

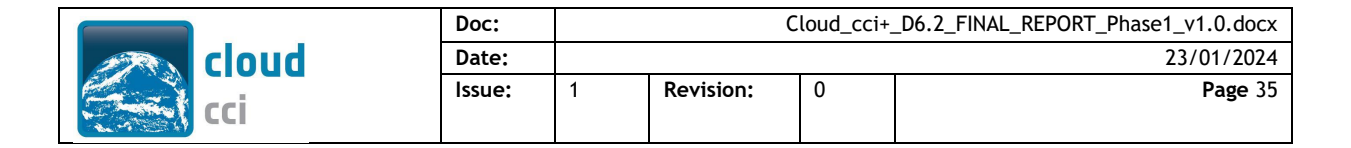
6 Definitions, Acronyms, Abbreviations

AATSR	Advanced Along Track Scanning Radiometer	
ATBD	Algorithm Theoretical Basis Document	
ATSR	Along-Track Scanning Radiometer	
AVHRR	Advanced Very High Resolution Radiometer	
CEDA	British Atmospheric Data Centre	
BRDF	Bidirectional Reflectance Distribution Function	
CALIPSO	Cloud-Aerosol Lidar and Infrared Pathfinder Satellite Observations	
CFMIP	Cloud Feedback Model Intercomparison Project	
CM	Configuration Management	
CMIP	Climate Model Intercomparison Project	
CM SAF	EUMETSAT Satellite Application Facility on Climate Monitoring	
COSP	CFMIP Observational Simulator Package	
DARDAR	raDAR/liDAR	
DISORT	Discrete Ordinates Radiative Transfer	
DWD	Deutscher Wetterdienst	
EC-EARTH	Earth system climate modelling version of the ECMWF model	
ECMWF	European Centre for Medium Range Weather Forecast	
ECSS	European Cooperation for Space Standardization	
ECV	Essential Climate Variable	
EO	Earth Observation	
EOS	Earth Observing System	
ESA	European Space Agency	
EUMETSAT	European Organization for the Exploitation of Meteorological Satellites	
FCDR	Fundamental Climate Data Record	
GCM	Global Circulation Model	
GCOS	Global Climate Observing System	
GERB	Geostationary Earth Observation Budget Instrument	
GEWEX	Global Energy and Water Cycle Experiment	
GRAPE	Global Retrieval of ATSR cloud Parameters and Evaluation	
GSICS	Global Space-based Inter-Calibration System	
GTS	Global Telecommunication System	
IPCC	International Panel on Climate Change	
IR	Infrared	
К	Kelvin	
MODIS	Moderate Resolution Imaging Spectroradiometer	
MSG	Meteosat Second Generation	
MTG	Meteosat Third Generation	
NASA	National Aeronautics and Space Administration	
NERC	Natural Environment Research Council	
	NERC Earth Observation Data Centre	
CEDA	.,	



Doc:		Cloud_cci+_D6.2_FINAL_REPORT_Phase1_v1.0.docx			
Date:				23/01/2024	
Issue:	1	Revision:	0	Page 34	

NIR	Near Infrared
NOAA	National Oceanic & Atmospheric Administration
NWP	Numerical Weather Prediction
OE	Optimal Estimation
OLR	Outgoing Longwave Radiation
ORAC	Oxford RAL Aerosol and Cloud
UO	University of Oxford
PUG	Product User Guide
PVP	Product Validation Plan
PVIR	Product Validation and Intercomparison Report
RAL	Rutherford Appleton Laboratory
RTM	Radiative Transfer Model
RTTOV	Radiative Transfer for TOVS
SAF	Satellite Application Facility
SCOPE-CM	Sustained and Coordinated Processing of Environmental Satellite Data for Climate Monitoring
SEVIRI	Spinning Enhanced Visible and Infrared Imager
SLSTR	Sea and Land Surface Temperature Radiometer
SOW	Statement Of Work
SST	Sea Surface temperature
SVR	System verification Report
TCDR	Thematic Climate Data Record
TIR	Thermal Infrared
TR	Technical Requirement
WCRP	World Climate Research Program
WMO	World Meteorology Organisation



Annex A - Architecture of the Cloud_cci processing environment

There are two processing centres/facilities in Cloud_cci used for the production of the v1 datasets:

- Operating facilities at DWD (including ECMWF facility); CC4CL
- Operating facility at RAL; CC4CL

The Cloud_cci system uses not only resources at these three institutes but also at ECMWF as well with interfaces between all centres. The Cloud_cci project has made use of this distributed environment considering the different focus and expertise of these institutes and allocating additional resources for processing. With the presented architecture, data streams are managed as effective as possible. The distributed processing environment of Cloud_cci is shown schematically in Figure A-1.

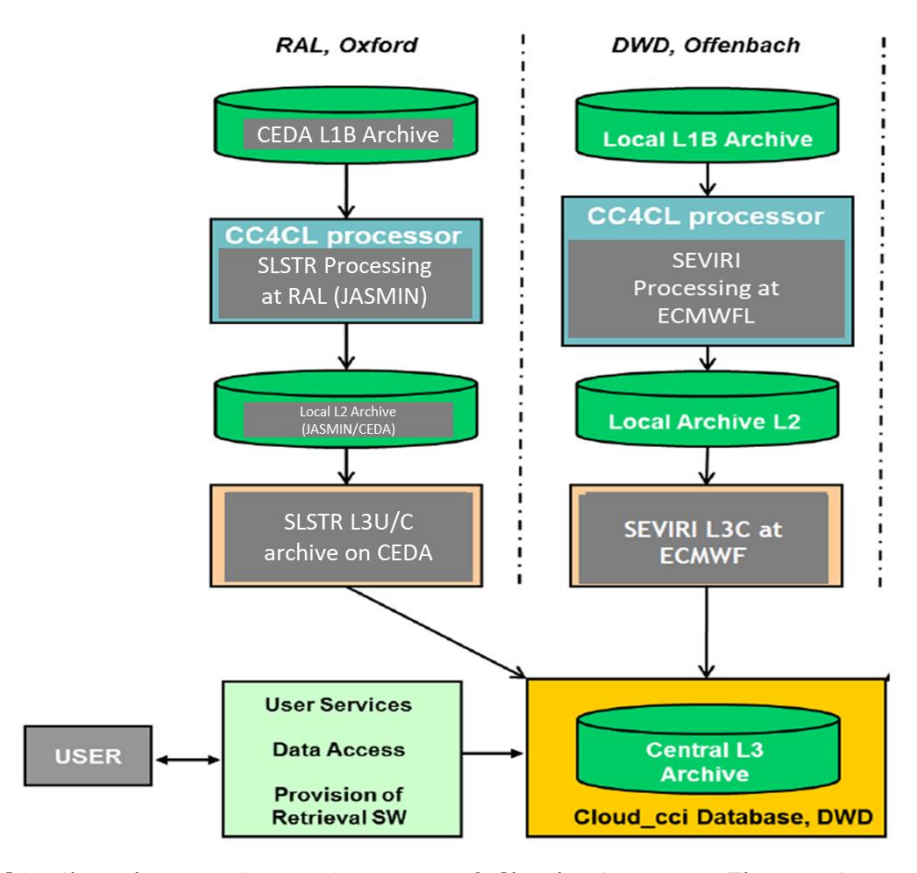


Figure A-1 Distributed processing environment of Cloud_cci system. There exist two processing centres at which the CC4CL processor is implemented and run.

The input data (Level-1 and auxiliary) and intermediate products were filed at the respective processing centres RAL and DWD. Level-2 output of the processors were stored at the respective processing centre and subsequently used to generated Level-3U and Level-3C products (see Table 3-5 for a description of the different processing levels). For this data version, only two months were processed. Level-2 und Level-3 products are collected at DWD for storage.

The Cloud_cci processing systems are built modularly. The processing software and hardware configuration is maintained under version control to ensure consistency and repeatability of the output products. Controlled error handling and appropriate QC procedures are implemented. More information about the Systems Specification and processing systems can be found in SSDv5.